

Can quarkonia survive deconfinement?

Ágnes Mócsy*

RIKEN-BNL Research Center, Brookhaven National Laboratory, Upton, New York 11973, USA

Péter Petreczky†

RIKEN-BNL Research Center and Physics Department, Brookhaven National Laboratory, Upton, New York 11973, USA
(Received 18 May 2007; revised manuscript received 2 October 2007; published 9 January 2008)

We study quarkonium correlators and spectral functions at zero and finite temperature in QCD with only heavy quarks using potential models combined with perturbative QCD. First, we show that this approach can describe the quarkonium correlation function at zero temperature. Using a class of screened potentials based on lattice calculations of the static quark-antiquark free energy we calculate spectral functions at finite temperature. We find that all quarkonium states, with the exception of the $1S$ bottomonium, dissolve in the deconfined phase at temperatures smaller than $1.5T_c$, in contradiction with the conclusions of recent studies. Despite this the temperature dependence of the quarkonium correlation functions calculated on the lattice is well reproduced in our model. We also find that even in the absence of resonances the spectral function at high temperatures is significantly enhanced over the spectral function corresponding to free quark-antiquark propagation.

DOI: [10.1103/PhysRevD.77.014501](https://doi.org/10.1103/PhysRevD.77.014501)

PACS numbers: 11.15.Ha, 12.38.Aw

I. INTRODUCTION

The study of quarkonia at finite temperature is interesting for several reasons. First, due to their small size, these heavy quark-antiquark bound states provide a bridge between perturbative and nonperturbative quantum chromodynamics (QCD), testing forces at intermediate distances. At high temperatures, color screening, which is usually understood in terms of in-medium modification of interquark forces, occurs. Based on this Matsui and Satz argued that above the transition temperature T_c screening effects are strong enough to lead to dissolution of the J/ψ state. This can then be used as a signal of quark-gluon plasma formation in heavy ion collisions [1].

Because of the large quark mass $m = m_{c,b} \gg \Lambda_{\text{QCD}}$, the velocity v of heavy quarks in the bound state is small, and the binding effects in quarkonia at zero temperature can be understood in terms of a nonrelativistic potential model with a Coulomb plus linear form, known as the Cornell potential [2–5]. Potential models appeared to be very successful in describing the quarkonium spectrum and have been extensively used in the past 20 years, see Ref. [6]. More recently, an understanding has developed on how to derive the potential models from QCD using a sequence of effective field theories: nonrelativistic QCD (NRQCD), an effective theory where all modes above the scale m are integrated out, and potential nonrelativistic QCD (pNRQCD), an effective theory in which all modes above the scale mv are integrated out [7,8]. The concept of the potential can be given a solid field theoretical definition in this framework at any order of perturbation theory. In particular, the quark-antiquark potential is defined in terms

of the expectation value of the Wilson loops. Relativistic corrections to the potential can also be calculated. They are expressed in terms of the Wilson loops with appropriate insertions of electric and magnetic fields, see Refs. [9–11].

Based on the success of the potential model at zero temperature, and the idea that color screening implies modification of the interquark forces, attempts to understand quarkonium properties at finite temperature using potential models have been made [1,12–14]. While in these works phenomenological potentials have been used, more recent studies went one step further and attempted to connect the potential to lattice calculations of the finite temperature free energy of a static quark-antiquark pair [15–22].

Quarkonium states at zero temperature are well defined: their widths are very small compared to their binding energies, at least for states below the threshold. At finite temperature the situation is different. We expect that all quarkonium states will acquire a sizable width, which increases with increasing temperature. At some temperature the width becomes large enough that it is no longer meaningful to talk about individual quarkonium states. Instead, one should consider the spectral function, which contains contributions from all possible states in a channel with given quantum numbers. Furthermore, the spectral function in the vector channel is a quantity which can be measured directly since it is proportional to the dilepton production rate. Quarkonium spectral functions at finite temperature have been considered only relatively recently. Using lattice QCD, charmonium correlators have been calculated and the corresponding spectral functions have been extracted using the maximum entropy method (MEM) [23–30]. Although this approach can in principle provide the ultimate solution to the problem of in-medium quarkonium properties, current calculations have serious

*mocsy@bnl.gov

†petreczk@bnl.gov

limitations and cannot give detailed information about quarkonium spectral functions. Using the MEM at zero temperature one can reconstruct the basic features of the spectral functions: the ground state, the excited states, and the continuum [30]. Individual excited states, however, cannot be resolved. At finite temperature, even resolving the ground state appears to be difficult with existing lattice data. The only statement that can be made at this time is that in the pseudoscalar channel, quarkonium spectral functions do not show significant changes up to temperatures as high as $1.5T_c$, while in the scalar channel the spectral function is strongly modified just above the transition temperature [30].

For this reason, quarkonium correlation functions have been studied using a simplified model of the spectral function, which contained bound states and a perturbative continuum [31,32]. The results of these calculations have been compared to lattice results and no agreement has been found. Very recently this approach has been extended using the full nonrelativistic Green's function of heavy quark-antiquark pairs to estimate the spectral function and the corresponding Euclidean correlators [21,22,33]. However, even in these approaches no agreement with lattice calculations has been found.

In the present paper we study spectral functions in the pseudoscalar, vector, scalar, and axial-vector channels which correspond to η_c (η_b), J/ψ (Υ), χ_{c0} (χ_{b0}), and χ_{c1} (χ_{b1}) charmonium (bottomonium) states, respectively. In the energy region below and near the continuum threshold the spectral function is calculated using a potential model and nonrelativistic Green's function. Since the potential at finite temperature is not known, we consider a class of screened potentials based on lattice results on the static quark-antiquark free energy. Well above the threshold, the nonrelativistic spectral function is matched to the perturbative fully relativistic result. From this the Euclidean correlators are calculated. We then compare these correlators to the results of recent lattice calculations. We find that the lattice data does not necessarily imply survival of different quarkonium states. Rather, despite the fact that most quarkonia, with the exception of the 1S bottomonium, are dissolved at temperatures smaller than $1.5T_c$, agreement with the correlator data is found. Clearly, dissociation temperatures previously quoted in the literature (e.g. $2T_c$ for J/ψ) have not been seen in our analysis.

The rest of the paper is organized as follows: The framework for calculating quarkonium spectral functions is discussed in Sec. II. In Sec. III we show our analysis of the quarkonium spectral functions and Euclidean correlators at zero temperature and compare to lattice QCD results. Sections IV and V contain our results on the finite temperature spectral function and correlators. Finally, in Sec. VI we give our conclusions and outlook. The reader not interested in technical details can skip Secs. II and III. Further technical details of our calculations are presented in the Appendices.

II. QUARKONIUM SPECTRAL FUNCTIONS IN THE NONRELATIVISTIC LIMIT

In this section we discuss quarkonium spectral functions in the free theory as well as in the nonrelativistic limit. In what follows we consider the case of zero spatial momentum, i.e. quarkonium at rest. The spectral function is defined as the imaginary part of the retarded current-current correlator

$$\sigma(\omega) = -\frac{1}{\pi} \text{Im} D_R(\omega), \quad (1)$$

$$iD_R(\omega) = \int dt e^{i\omega t} \theta(t) \int d^3x \langle [j(t, \vec{x}), j(0, 0)] \rangle. \quad (2)$$

It carries information about all the possible states with a given quantum number, which is fixed by the current

$$j = \bar{q}\Omega q \quad (3)$$

with $\Omega = 1, \gamma_5, \gamma_\mu, \gamma_\mu \gamma_5$ for scalar, pseudoscalar, vector, and axial-vector channels, respectively.

For large ω the spectral function can be calculated in perturbation theory (see e.g. [34,35])

$$\sigma(\omega) = \frac{N_c}{8\pi^2} \omega^2 \left(a + b \frac{s_0^2}{\omega^2} \right) \sqrt{1 - \frac{s_0^2}{\omega^2}} \left(1 + C \frac{\alpha_s}{\pi} \right). \quad (4)$$

Here $a = 1, b = 0$ for pseudoscalar, $a = 2, b = 1$ for vector, $a = 1, b = -1$ for the scalar, and $a = 2, b = -3$ in the axial-vector channel, respectively. In leading order perturbation theory the threshold is $s_0 = 2m_{c,b}$. The coefficient C of the leading perturbative correction has been calculated only for the massless case [36]. The number of colors in QCD is $N_c = 3$.

While perturbation theory is reliable away from the threshold, $\omega \gg s_0$, the physics becomes quite complicated near the threshold, even in the weak coupling regime [37–40]. Close to the threshold the quark and antiquark move slowly allowing enough time for multiple gluon exchange. Adding an extra gluon exchange does not lead to a suppression by α_s . In this case we need to resum ladder diagrams. In the following we discuss this resummation separately for the pseudoscalar and scalar channels. The vector channel has been discussed in detail in Ref. [39], while the axial-vector channel is completely analogous to the scalar case.

A. Pseudoscalar channel

The summation of ladder diagrams corresponds to solving the integral equation for the vertex function

$$\Gamma(p, q) = \gamma_5 + \int \frac{d^4k}{(2\pi)^4} S_F\left(k + \frac{q}{2}\right) \Gamma(k, q) S_F\left(k - \frac{q}{2}\right) \times \tilde{V}(p - k) \quad (5)$$

and inserting the solution of this equation into the 1-loop

expression of the meson correlator (see e.g. [39])

$$D(q^2) = N_c \int \frac{d^4 p}{(2\pi)^4} \text{Tr} \left[S_F \left(p + \frac{q}{2} \right) \Gamma(p, q) S_F \left(p - \frac{q}{2} \right) \gamma_5 \right]. \quad (6)$$

In general this task is complicated, but it simplifies considerably in the nonrelativistic limit. In this case following Ref. [39] we can replace the quark propagators with the corresponding nonrelativistic forms

$$S_F \left(p + \frac{q}{2} \right) = \frac{(1 + \gamma_0)m + \gamma_0(p_0 + E/2) + \vec{\gamma} \cdot \vec{p}}{2m(\frac{E}{2} + p_0 - \frac{\vec{p}^2}{2m} + i\epsilon/2)}, \quad (7)$$

$$S_F \left(p - \frac{q}{2} \right) = \frac{(1 - \gamma_0)m + \gamma_0(p_0 - E/2) + \vec{\gamma} \cdot \vec{p}}{2m(\frac{E}{2} - p_0 - \frac{\vec{p}^2}{2m} + i\epsilon/2)}.$$

Here we have taken into account that $q = (2m + E, \vec{0})$ and $E \ll 2m$. The 1-gluon exchange operator in this limit is $\tilde{V}(\vec{k} - \vec{p}) \equiv V(|\vec{k} - \vec{p}|) = \frac{4}{3} \alpha_s 4\pi D_{00}(|\vec{k} - \vec{p}|)$, where D_{00} is the temporal Coulomb gauge gluon propagator. In this limit the vertex function can be chosen to be independent of p_0 [39].

The leading order result for the pseudoscalar spectral function can be obtained by replacing $\Gamma = \gamma_5$ in Eq. (6) and using the nonrelativistic form of the quark propagators above with only the first term in the denominator. The retarded nature of the meson correlator $D(q^2)$ is ensured by the $+i\epsilon$ prescription in the quark propagators. This gives for the free nonrelativistic spectral function

$$\sigma(E) = -\frac{1}{\pi} \text{Im} D(q^2) = \frac{N_c}{2\pi^2} m^{3/2} E^{1/2}. \quad (8)$$

Note, that this result can also be obtained from Eq. (4) by writing $\omega = 2m + E$ and $s_0 = 2m$, and expanding in E/m to leading order.

Defining the scalar function

$$\frac{(1 + \gamma_0)}{2} \Gamma(\vec{p}, E) \frac{(1 - \gamma_0)}{2} = \frac{(1 + \gamma_0)}{2} \gamma_5 \frac{(1 - \gamma_0)}{2} \tilde{\Gamma}(\vec{p}, E) \quad (9)$$

and performing the integral over k_0 explicitly, the integral equation for the vertex function can be written as

$$\tilde{\Gamma}(\vec{p}, E) = 1 + \int \frac{d^3 k}{(2\pi)^3} \frac{1}{E + i\epsilon - k^2/m} V(|\vec{p} - \vec{k}|) \tilde{\Gamma}(\vec{k}, E). \quad (10)$$

By introducing the nonrelativistic Green's function

$$G^{nr}(\vec{k}, E + i\epsilon) = -\frac{1}{E + i\epsilon - \frac{k^2}{m}} \tilde{\Gamma}(\vec{k}, E), \quad (11)$$

the equation for the scalar vertex function $\tilde{\Gamma}(\vec{k}, E)$ can be rewritten in the form

$$-(E + i\epsilon - \frac{p^2}{m}) G^{nr}(\vec{p}, E + i\epsilon) = 1 - \int \frac{d^3 k}{(2\pi)^3} V(|\vec{p} - \vec{k}|) G^{nr}(\vec{k}, E + i\epsilon), \quad (12)$$

which is the Schrödinger equation in momentum space. In a more familiar form, in coordinate space, it reads

$$\left[-\frac{1}{m} \vec{\nabla}^2 + V(r) - (E + i\epsilon) \right] G^{nr}(\vec{r}, \vec{r}', E + i\epsilon) = \delta^3(r - r'). \quad (13)$$

Here

$$G^{nr}(\vec{r}, \vec{r}', E + i\epsilon) = \int \frac{d^3 k}{(2\pi)^3} e^{-i\vec{k} \cdot (\vec{r} - \vec{r}')} G^{nr}(\vec{k}, E + i\epsilon) \quad (14)$$

is the nonrelativistic Green's function in coordinate space and

$$V(r) = \int \frac{d^3 k}{(2\pi)^3} V(|\vec{k}|) e^{-i\vec{k} \cdot \vec{r}} \quad (15)$$

is the potential. Thus we can write

$$\begin{aligned} \sigma(E) &= \frac{2N_c}{\pi} \text{Im} \int \frac{d^3 k}{(2\pi)^3} G^{nr}(\vec{k}, E + i\epsilon) \\ &= \frac{2N_c}{\pi} \text{Im} G^{nr}(\vec{r}, \vec{r}', E + i\epsilon) \Big|_{\vec{r}=\vec{r}'=0}. \end{aligned} \quad (16)$$

Therefore, in order to calculate the pseudoscalar spectral function in the nonrelativistic limit we have to solve the Schrödinger equation (13) for $G^{nr}(\vec{r}, \vec{r}', E + i\epsilon)$ and take the limit $\vec{r} = \vec{r}' = 0$, according to (16).

B. Scalar channel

The calculation of the scalar spectral function is somewhat more complicated. To understand the problem better, let us consider the noninteracting case first. From the structure of the quark propagators in the nonrelativistic limit it is clear that for the scalar vertex $\Omega = 1$ the meson correlator is equal to zero in leading order of a $1/m$ expansion (cf. Eqs. (7)). Therefore the second and third terms in the numerator of Eqs. (7) should be retained. We then get

$$\begin{aligned} D(q^2) &= N_c \int \frac{d^4 p}{(2\pi)^4} \\ &\times \frac{\frac{\vec{p}^2}{m^2} - E/m}{(\frac{E}{2} + p_0 + i\frac{\epsilon}{2} - \frac{\vec{p}^2}{2m})(\frac{E}{2} + p_0 + i\frac{\epsilon}{2} - \frac{\vec{p}^2}{2m})}. \end{aligned} \quad (17)$$

Taking the imaginary part and performing the integral we get

$$\sigma(E) = \frac{N_c}{2\pi^2} m^{1/2} E^{3/2}. \quad (18)$$

Note that we arrive at the same result if we consider the nonrelativistic scalar vertex $\Omega = \frac{\vec{\gamma} \cdot \vec{p}}{m}$ instead of the relativistic one $\Omega = 1$. In fact, this type of nonrelativistic vertex is used to study the $\chi_{c,b}$ states in NRQCD [41,42].

Repeating all the steps discussed in the previous section we write the correlator

$$D(q^2) = N_c \int \frac{d^4 p}{(2\pi)^4} \text{Tr} \left[S_F \left(p + \frac{q}{2} \right) \Gamma(p, q) \right. \\ \left. \times S_F \left(p - \frac{q}{2} \right) \frac{\vec{\gamma} \cdot \vec{p}}{m} \right], \quad (19)$$

where the vertex function $\Gamma(p, q)$ satisfies the equation

$$\Gamma(p, q) = \frac{\vec{\gamma} \cdot \vec{p}}{m} + \int \frac{d^4 k}{(2\pi)^4} S_F \left(k + \frac{q}{2} \right) \Gamma(k, q) S_F \left(k - \frac{q}{2} \right) \\ \times V(p - k). \quad (20)$$

Introducing the scalar function

$$\frac{(1 + \gamma_0)}{2} \Gamma(p, q) \frac{(1 - \gamma_0)}{2} = \frac{(1 + \gamma_0)}{2} \frac{\vec{\gamma} \cdot \vec{p}}{m} \\ \times \frac{(1 - \gamma_0)}{2} \tilde{\Gamma}(\vec{p}, E), \quad (21)$$

we write

$$D(q^2) = \int \frac{d^3 k}{(2\pi)^3} \frac{1}{E + i\epsilon - k^2/m} \tilde{\Gamma}(\vec{k}, E) \frac{\vec{k}^2}{m^2}. \quad (22)$$

It is easy to see that $\tilde{\Gamma}(\vec{k}, E)$ satisfies Eq. (12) and therefore we can write

$$\sigma(E) = -\frac{1}{\pi} \text{Im} D(q^2) \\ = \frac{2N_c}{\pi} \frac{1}{m^2} \text{Im} \vec{\nabla} \cdot \vec{\nabla}' G^{nr}(\vec{r}, \vec{r}', E + i\epsilon)|_{\vec{r}=\vec{r}'=0}. \quad (23)$$

Thus to calculate the spectral function in the scalar channel, we have to calculate the derivatives of the nonrelativistic Green's function with respect of \vec{r} and \vec{r}' and take then the limit $\vec{r} = \vec{r}' = 0$, according to (23).

C. Numerical solution of the Schrödinger equation

To obtain the spectral function in the nonrelativistic limit, we have to solve Eq. (13) for nonzero ϵ , i.e. complex energy. We use the numerical method developed in Ref. [39] for this purpose which we have extended to incorporate the scalar channel, as discussed in Appendix A. At finite temperature all particles have a thermal width, but for heavy quarks this is expected to be small. Therefore in our study we aim to get the Green's function in the limit $\epsilon \rightarrow 0$. In the numerical analysis we used $\epsilon_c = 0.03m_c$, $0.01m_c$, and $0.005m_c$ for charmonium,

and $\epsilon_b = 0.009m_b$, $0.003m_b$, and $0.0015m_b$ for bottomonium. For the continuum part of the spectral function all three values of the width ϵ give the same result. In the low energy part the shape of the spectral function agrees quite well for the smallest two $\epsilon_{c,b}$ values. In what follows, we will show spectral functions calculated for $\epsilon_c = 0.005m_c$ and $\epsilon_b = 0.0015m_b$. We note that for bound states close to the threshold even a tiny width could have a significant effect, namely, it could eliminate the bound state peak in the spectral function. But on the level of correlators this introduces at most a 1% effect.

For the numerical analysis we need to specify the potential in Eq. (13). The Cornell parametrization of the potential turned out to be very successful for the phenomenological description of the quarkonium spectra, as well as a fit Ansatz for the lattice data on quark-antiquark potential. To include medium effects at high temperatures, as well as many-body effects at zero temperature (e.g. threshold for open charm or beauty production, and quarkonia plus glueball production) we will use the following parametrization of the potential

$$V(r) = \begin{cases} -\frac{\alpha}{r} + \sigma r, & r < r_{\text{med}} \\ -\frac{\alpha'}{r} e^{-\mu r} + \frac{\sigma'}{\mu} (1 - e^{-\mu r}) + V_0, & r > r_{\text{med}} \end{cases}. \quad (24)$$

The parameters α and σ are fixed by zero temperature lattice QCD calculations, while other parameters may be temperature dependent. We discuss the choice of these parameters in the following sections. The potential used in the numerical analysis is of course smooth. We used a Fermi-Dirac function to interpolate between the two forms in Eq. (24) at $r = r_{\text{med}}$. At finite temperature we also used a more complicated interpolation between the short and long distance behavior (see Sec. IV and Appendix C). Above deconfinement the singlet free and internal energies of the static quark-antiquark pair have also been used as a potential.

III. QUARKONIUM CORRELATORS AT ZERO TEMPERATURE

In this section we discuss quarkonium correlators obtained from the spectral functions, which are calculated using a potential model matched onto the perturbative QCD results at higher energies.

From the spectral function, determined as discussed in Sec. II, we calculate the Euclidean correlators defined by

$$G(\tau, T) = \int_0^\infty d\omega \sigma(\omega, T) K(\omega, \tau, T). \quad (25)$$

At zero temperature, $K(\omega, \tau, T) = \exp(-\omega\tau)$. We compare the calculated correlators to recent numerical results calculated from isotropic [25] and anisotropic [30] lattice formulations.

A. Numerical analysis of the spectral functions in the nonrelativistic limit

Using Eqs. (16) and (23) we calculate the pseudoscalar and scalar spectral functions in the nonrelativistic approximation. To do this, we have to specify the parameters of the potential α , σ , r_{med} , μ , α' , σ' , and V_0 , as well as the charm and bottom quark masses $m_{c,b}$. In this work we are interested in QCD with only heavy quarks because most of the calculations are performed in the quenched approximation. In quenched QCD (pure SU(3) gauge theory) the static quark-antiquark potential is well known. In particular, lattice calculations of the potential have been extrapolated to the continuum limit [43]. It turns out that for distances $r > 0.4$ fm an excellent description of the potential calculated on the lattice can be given by the Cornell parametrization with $\alpha = \pi/12$ and $\sigma = (1.65 - \pi/12)r_0^{-2}$. Here r_0 is the Sommer parameter defined as

$$r^2 \frac{d^2 V}{dr^2} \Big|_{r=r_0} = 1.65. \quad (26)$$

As is done in most of the quenched QCD studies, we use the phenomenological value of the Sommer parameter $r_0 = 0.5$ fm. The Cornell parametrization with the above parameters gives a fairly good description of the lattice data, even at short distances down to 0.1 fm. Only at distances $r < 0.1$ fm the effect of the running coupling appear to be important [44]. Therefore the Cornell parametrization is appropriate for describing the quarkonium spectrum, which is sensitive to the potential in the region $0.1 \text{ fm} < r < 1 \text{ fm}$. The charm and bottom quark masses are chosen such that the potential model reproduces the quenched lattice data on charmonium [45] and bottomonium spectra [46]. Since the NRQCD calculation of Ref. [46] does not give the absolute value of the bottomonium masses, we require that the mass of η_b is equal to 9.4 GeV. In Table I, we show the masses of different quarkonium states and the values of the quark masses. In Fig. 1 we show the quarkonium spectral function in the pseudoscalar channel for three different sets of the parameters μ and r_{med} . The potential (24) corresponding to these parameter sets is shown in Fig. 2. Here we use $\alpha' = \alpha$ and

TABLE I. Charmonium and bottomonium masses in MeV calculated in our model and in quenched lattice simulations. The values of the charm and bottom quark masses in our model are also shown.

Charmonia			Bottomonia		
$m_c = 1.19 \text{ GeV}$			$m_b = 4.575 \text{ GeV}$		
State	Model	Lattice	State	Model	Lattice
1^1S_0	3030	3012(1)	1^1S_0	9406	9400
1^3S_1	3030	3084(1)	1^3S_1	9406	9426(4)
1^3P_0	3437	3408(9)	1^3P_1	9736	9800(16)
2^1S_0	3675	3739(46)	2^3S_1	9874	9938(21)
2^3P_0	3966	4008(122)	2^1P_1	10 100	10 181(64)

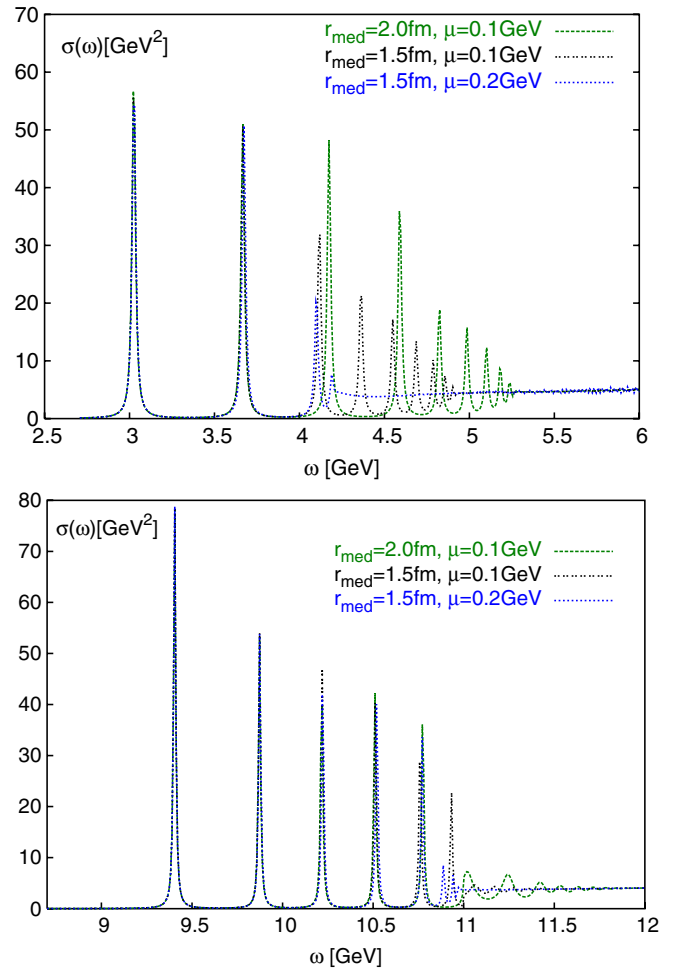


FIG. 1 (color online). The nonrelativistic pseudoscalar spectral functions calculated for charmonium (top) and bottomonium (bottom) using the screened Cornell potential.

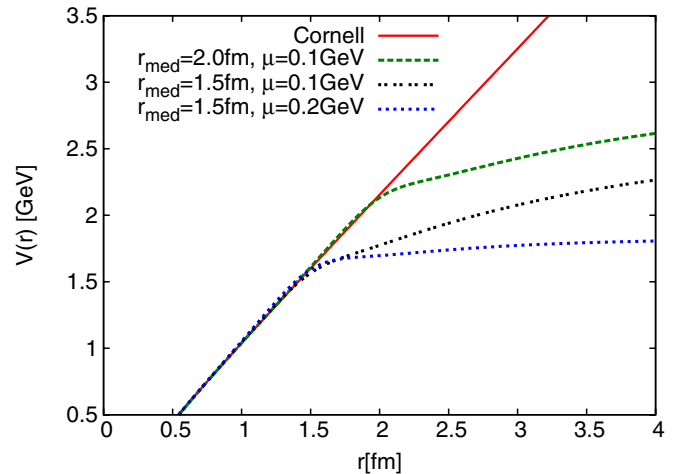


FIG. 2 (color online). The potential at $T = 0$ for different parameters.

$\sigma' = \sigma$. In QCD with only heavy quarks, string breaking does not occur until distances where the potential becomes comparable with twice the heavy quark mass. However, as the energy ω is increased the distance between bound state peaks becomes very small (as can already be seen in Fig. 1). Furthermore, at even larger energy, it is possible to create quarkonium plus glueball states which subsequently decay into quarkonium states. In this energy regime, it is impossible to discriminate between individual states and thus the spectral function will have a continuum. This will happen at energies of about $\omega \simeq 4\text{--}5$ GeV for charmonium and 11 GeV for bottomonium. In this energy region the potential model, strictly speaking, will break down, but the effect of the interaction will still be important. To mimic the continuum part of the spectral functions, we will choose μ and r_{med} such that above energies 4–5 GeV for charmonium and 11 GeV for bottomonium, the corresponding spectral functions have a continuum. As we will see in the next section, the correlation function is not very sensitive to the exact choice of μ and r_{med} as long as the continuum threshold is larger than 4 GeV for charmonium and 11 GeV for bottomonium, as shown in Fig. 1. This figure illustrates that in the range studied, since the potential is only modified at distances larger than 1.5 fm, the lowest lying states are not affected by the choice of the parameters r_{med} and μ . In summary, many-body effects in the spectral function can be simulated by the screened Cornell potential given by Eq. (24) with appropriately chosen μ and r_{med} . As it is discussed in the next subsection this somewhat *ad hoc* treatment of many-body effects has almost no effect on the correlation functions in Euclidean time. The width of the quarkonium states in the spectral functions shown in Fig. 1 are a numerical artifact due to the nonzero value of the parameter $\epsilon_{c,b}$. As mentioned in the previous section, however, this parameter does not have a visible effect on the correlation function.

B. Direct comparison of the correlation functions with lattice data

The main focus of this paper is to study the temperature dependence of the correlation function. For this the form of the zero temperature correlator is not crucial. To ensure, however, that the comparison of the lattice data and the potential model is meaningful, it is desirable to show that the correlation functions calculated in the model agree at least semiquantitatively with the lattice data. In this subsection we compare the correlators from the model calculations to the lattice data at zero temperature. Quarkonium correlators have been studied in isotropic and anisotropic lattice formulations. The correlators of the meson currents calculated on the lattice require renormalization. The corresponding renormalization constants have been calculated for isotropic lattices only: see discussion in Refs. [25,27,28]. Therefore, for comparison with our model predictions, we use the data obtained on isotropic

lattices [25]. We use the value of the renormalization constants given in Ref. [25]. In the case of charmonium, we compare our calculations to the new lattice calculation on a $48^3 \times 64$ lattice at $\beta = 6/g^2 = 7.192$ [47]. In the bottomonium case, we compare our calculations to the lattice data of Ref. [28]. In these studies the quark masses, and thus the meson masses, were larger than their physical value. For this reason, we repeat the analysis from the previous section using larger quark masses. In Table II we give the resulting quarkonium masses as well as the corresponding charm and bottom quark mass. In the present analysis, we use $r_0 = 0.5$ fm as well as the interpolation formula for r_0 in the gauge coupling β given in Ref. [43] to set the scale. As a consequence the value of the lattice spacing is smaller; we get $a = 0.017$ fm for the lattice spacing at $\beta = 7.192$. Because of this, the meson masses are larger than those quoted in Ref. [25], where the value of the string tension $\sqrt{\sigma} = 425$ MeV was used to set the scale.

The relation between the spectral function and the non-relativistic Green's function discussed in Sec. II holds only at leading order. It will be modified by radiative and relativistic corrections. The radiative corrections, in particular, turn out to be quite large [48–50]. To take into account these corrections we introduce K factors. These are determined such that the large τ behavior of the correlators calculated in our model matches the lattice data, i.e. we assume

$$\sigma(\omega) = K \frac{2N_c}{\pi} \text{Im} G^{nr}(0, 0, E + i\epsilon) \quad (27)$$

for the S -wave quarkonia and similar relation between the derivative of the Green's function for the P -wave quarkonia. The values of K are given in Table I for each channel. For the study of the temperature dependence of the correlator, which is the main objective of this paper, omitting K would have an effect on the ratio G/G_{rec} which is smaller than 0.1%.

It is important to be aware that the nonrelativistic approximation breaks down at large enough energies. On the other hand, for large energy, the perturbative result for the spectral function given in Eq. (4) becomes reliable. Therefore the nonrelativistic spectral function in Eq. (27)

TABLE II. Charmonium and bottomonium masses in MeV from isotropic lattice calculations compared with the masses calculated in our model. Also shown are the K -factors for the nonrelativistic spectral functions.

State	Charmonia $m_c = 1.7$ GeV			Bottomonia $m_b = 5.8$ GeV			
	Model	Lattice	K	State	Model	Lattice	K
1^1S_0	3936	4023(52)	2.0	1^1S_0	11 790	11 820(81)	1.8
1^3S_1	3936	4129(105)	0.8	1^3S_1	11 790	11 886(81)	1.38
1^3P_0	4319	4543(207)	2.0	1^3P_0	12 120	12 295(324)	2.7

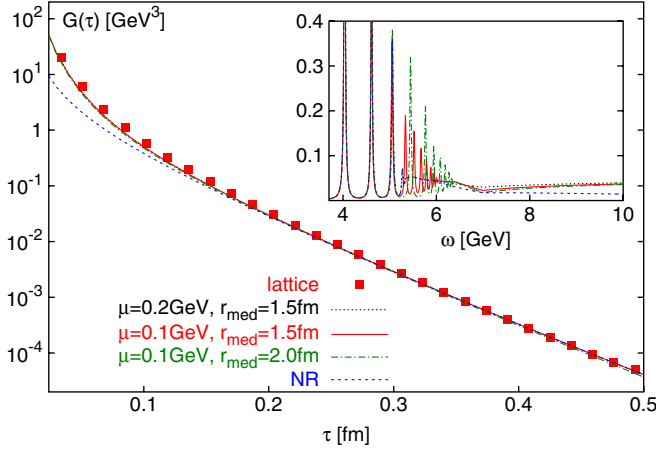


FIG. 3 (color online). The pseudoscalar charmonium correlator calculated in our model and compared to lattice data of Ref. [25]. In the inset, the corresponding spectral functions $\sigma(\omega)/\omega^2$ are shown.

has been smoothly matched onto the perturbative relativistic form given by Eq. (4) and $\alpha_s = 0.2$. In Fig. 3 we show the pseudoscalar charmonium correlators and the corresponding spectral functions calculated for different values of r_{med} and μ . The model calculation of the correlators show reasonable agreement with the lattice data, and the correlator does not depend on the values of r_{med} and μ . Furthermore, our calculations indicate that even if we use the unscreened Cornell potential, this causes a change in the correlation function of less than 0.5%. Therefore the *ad hoc* treatment of many-body effects discussed in the previous subsection appears to have almost no effect on the Euclidean correlators.

We have used several procedures to match smoothly the nonrelativistic function to the relativistic behavior at large energies, and have found that the differences in the Euclidean time correlator introduced by different procedures are less than 0.5%.

To obtain the correct τ dependence of the correlators at short distances, the relativistic form of the spectral function must be used. The nonrelativistic continuum leads to a correlator which is more than an order of magnitude smaller than the lattice data at short distances, see Fig. 3. In Appendix B we discuss the additional analysis of the behavior of the correlation function at $\tau < 0.1$ fm, showing that it is clearly dominated by the relativistic continuum contribution of the spectral functions. This contradicts the statements made recently in the literature [19,22], that the lattice correlator do not carry information about the continuum.

The analysis discussed above for the pseudoscalar charmonium correlator we repeated in the vector and scalar channels, as well as for the case of bottomonium. Also in these channels a reasonable agreement between the lattice data and the model calculations has been found.

Since the Euclidean correlators fall off rapidly with increasing τ it is difficult to judge the agreement between the lattice data and the model calculations only looking at Fig. 3. It is better to study the ratio of the correlators calculated on the lattice to the correlators calculated in our model. This comparison reveals some discrepancies between the lattice data and the model. These discrepancies are due to lattice artifacts (at short Euclidean time separation), the limited validity of the nonrelativistic approach, and in some cases due to the lack of fine-tuning of the K -factor, as discussed in Appendix B where we show the details of this analysis as well as our results in other channels.

C. Zero temperature spectral function as reference

In the previous subsection we have shown that the nonrelativistic spectral function scaled with proper factors, which take into account the relativistic and radiative corrections, and matched to the perturbative relativistic spectral function can give a fairly good description of the lattice data obtained at quark masses larger than the physical values. We have repeated the procedure described in the previous section for the physical value of the quark masses, namely $m_c = 1.19$ GeV and $m_b = 4.575$ GeV. In this analysis, we used the K -factors listed in Table II and $r_{\text{med}} = 1.5$ fm and $\mu = 0.2$ GeV. The calculated spectral function will serve as a reference against which the finite temperature results in the next sections will be compared.

IV. QUARKONIUM CORRELATORS AT FINITE TEMPERATURE

As the temperature is increased, quarkonium spectral functions will change. This eventually results in a temperature dependence of the Euclidean correlator $G(\tau, T)$. However, the temperature dependence of $G(\tau, T)$ is also caused by the temperature dependence of the integration kernel in Eq. (25), which at finite temperature has the form

$$K(\omega, \tau, T) = \frac{\cosh \omega(\tau - 1/(2T))}{\sinh(\omega/(2T))}. \quad (28)$$

To separate out the trivial temperature dependence due to the integration kernel following Ref. [25], we calculate the reconstructed correlator

$$G_{\text{rec}}(\tau, T) = \int_0^\infty d\omega \sigma(\omega, T=0) K(\omega, \tau, T) \quad (29)$$

and study the ratios $G(\tau, T)/G_{\text{rec}}(\tau, T)$. If the spectral function does not change across the deconfinement phase transition this ratio will be unity and independent of the temperature. In this section we discuss the pseudoscalar and scalar channels in detail. In the scalar channel, there is a zero-mode contribution above the deconfinement temperature, i.e. there is a term proportional to $\omega \delta(\omega)$ in the

spectral function [51]. This contribution is not present in the derivative $G'(\tau, T)$ of the correlator $G(\tau, T)$ with respect to τ . Therefore, in the scalar channel we will consider the ratios of the derivatives $G'(\tau, T)/G'_{\text{rec}}(\tau, T)$ instead of $G(\tau, T)/G_{\text{rec}}(\tau, T)$.

A. Correlators in the free case

At sufficiently high temperatures all quarkonium states will melt and the interaction between the heavy quark and antiquark will be weak. In this limit, quarkonium spectral functions are well approximated by the leading perturbative (free field) expression

$$\sigma_{\text{free}}(\omega, T) = \frac{N_c}{8\pi^2} \omega^2 \left(a + b \frac{s_0^2}{\omega^2} \right) \tanh \frac{\omega}{4T} \sqrt{1 - \frac{s_0^2}{\omega^2}} \quad (30)$$

with $s_0 = 2m_{c,b}$. To obtain an estimate of the temperature dependence of the correlators, we calculate it using σ_{free} as the spectral function and consider the ratio G/G_{rec} . This should provide some upper bound on the size of the temperature dependence of the correlators. In Fig. 4, we show the ratios of the correlators and the ratios of their derivatives in the scalar channel. In the numerical analysis we have multiplied σ_{free} by the factor $1 + C\alpha_s/\pi$ used in Eq. (4) to mimic the leading perturbative corrections at large ω . This form of the continuum ensures that G/G_{rec} approaches one for small τ . As one can see from the figure, the correlators corresponding to free quark propagation are very different from the zero temperature correlators, namely, they are considerably smaller. The differences are considerably larger for bottomonium than for charmonium and slightly larger in the scalar channel than in the pseudoscalar one.

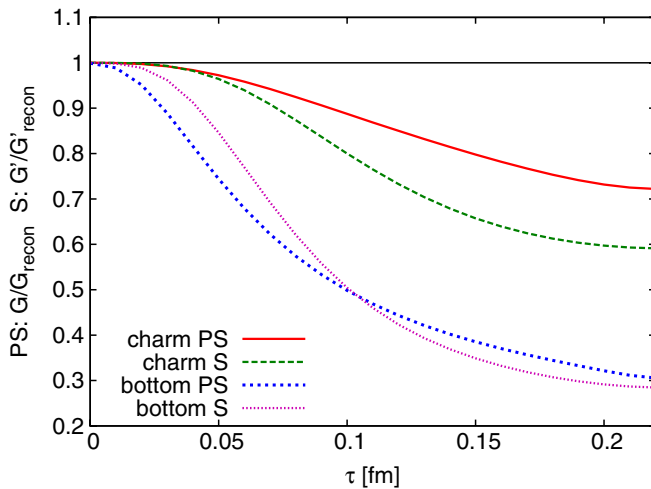


FIG. 4 (color online). The ratio G/G_{rec} for the pseudoscalar and G'/G'_{rec} for the scalar channels for charmonium and bottomonium.

B. Screening above deconfinement

Above the deconfinement temperature, we expect color screening to take place. The interaction between the heavy quark and the antiquark will be modified. We assume, however, that the integral Eq. (12) for the nonrelativistic Green's function still holds at finite temperature but with some temperature dependent potential $V(r, T)$. On the lattice color screening is studied by determining the correlation function of a color singlet static quark-antiquark pair separated by some distance r in Euclidean time, evaluated at $\tau = 1/T$. This is an expectation value of two Wilson lines

$$\text{Tr} \langle L(0)L^\dagger(r) \rangle = \exp(-F_1(r, T)/T) \quad (31)$$

and defines the so-called singlet free energy $F_1(r, T)$ [52]. Since this object is not gauge invariant, one has to calculate it in a fixed gauge. Most of the studies of screening of static quarks use the Coulomb gauge [44,53–57]. Instead of using the Coulomb gauge, one can insert a spatial transporter between the static quark and antiquark, i.e. calculate cyclic Wilson loops. Studies of cyclic Wilson loops at finite temperature have also been performed and have given results very similar to the Coulomb gauge calculations [58].

Studying $F_1(r, T)$ as a function of the separation r three different regions can be distinguished: the short distance region, the intermediate distance region, and the long distance region. At sufficiently short distances, F_1 is temperature independent and coincides with the zero temperature potential. In this region F_1 does not depend on the choice of the correlation function used to calculate it (e.g. Coulomb gauge correlator or cyclic Wilson loop). At some distance $r > r_{\text{med}}$, the singlet free energy becomes temperature dependent and deviates from the zero temperature potential. The r -dependence of the singlet free energy in this region depends on the choice of the correlation function (see discussion in Ref. [59]). The value of r_{med} separating the short and intermediate distance regions depends on the temperature as $r_{\text{med}}(T) = 0.43 \text{ fm}/(T/T_c)$ [60]. Finally at large distances, $rT > (1.0 - 1.25)$ the singlet free energy is exponentially screened [44]

$$F_1(r, T) = F_\infty(T) - \frac{4}{3} \frac{\alpha_1}{r} \exp(-\sqrt{4\pi\alpha_1}Tr). \quad (32)$$

This feature is independent of the choice of the operator. Moreover, $F_\infty(T)$ is universal and can be extracted from the gauge invariant Polyakov loop correlator $\langle \text{Tr} L(0)\text{Tr} L^\dagger(r) \rangle$ [53]. This gives the free energy of infinitely separated static quark-antiquark pairs $F_\infty(T)$ which is smaller than twice the self-energy of a heavy quark in the medium $V_\infty(T)$. This is because the free energy contains a negative entropy contribution $-TS_\infty(T)$ [53]. In fact this entropy contribution dominates at high temperatures, making $F_\infty(T)$ negative for $T > 3T_c$ [53]. We would expect that $\min(F_\infty(T), 0)$ is a lower bound on $V_\infty(T)$. Furthermore, for

this reason, at temperatures close to T_c the singlet free energy provides a lower bound on the potential in the sense that $V(r, T) > F_1(r, T)$.

We assume that the potential $V(r, T)$ shares the general properties of the singlet free energy discussed above, i.e. there is a short, intermediate, and long distance region. In the short distance region, $r < r_{\text{med}}(T)$ we assume that $V(r, T)$ is equal to the zero temperature potential. At large distances, $rT > 1.25$ we assume that $V(r, T)$ has the form

$$V(r, T) = V_\infty(T) - \frac{4}{3} \frac{\alpha_1}{r} \exp(-\sqrt{4\pi\tilde{\alpha}_1}Tr), \quad (33)$$

where α_1 and $\tilde{\alpha}_1$ were determined in [44]. In the case of a screened Cornell potential $V_\infty = \sigma/\mu$ (cf. Eq. (24)). In QCD with light dynamical quarks, string breaking occurs at distances of about 1 fm. Therefore, assuming $\mu \simeq 200$ MeV we estimate that $V_\infty = \sigma/\mu \simeq 1.1$ GeV, which agrees reasonably well with twice the binding energy of the heavy-light meson $2E_{\text{bind}} = 2M_{D,B} - 2m_{c,b}$. Using this analogy and realizing that the role of the effective screening mass in our case is taken by $1/r_{\text{med}}(T)$, we estimate $V_\infty(T) = r_{\text{med}}(T)\sigma$. This way we have specified the large distance behavior of the potential. In the intermediate distance range $r_{\text{med}}(T) < r < 1.25/T$ we use a Fermi-Dirac function to interpolate between the short and the long distance behavior, such that the value of the potential and its first derivative agree at $r = r_{\text{med}}$ and at $r = 1.25/T$. The potential constructed this way is shown in Fig. 5 for several different temperatures together with the lattice data on the singlet free energy. In Appendix C we give details about the construction of this potential. Let us note that the above choice of $V_\infty(T)$ is also motivated by recent model analysis of the singlet free energy with dimension two gluon condensate [61].

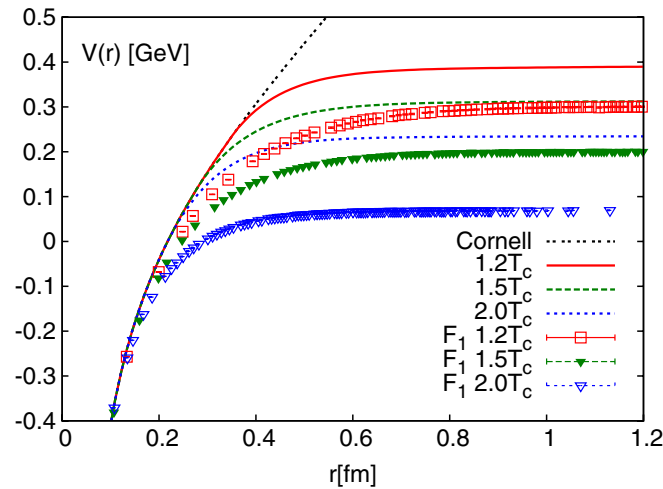


FIG. 5 (color online). The finite temperature potential used in our analysis at several values of the temperature together with the lattice data on the singlet free energy from Refs. [44,53,63].

C. Numerical results with $F_1(r, T)$

From the above discussion it is clear that the singlet free energy provides a lower limit for the screened potential. Therefore we have analyzed charmonium and bottomonium spectral functions using the singlet free energy as the potential $V(r)$ in Eq. (13). The numerical results for the charmonium spectral functions are shown in Fig. 6 (top) together with the corresponding correlation functions (inset). As one can see, all charmonium states are dissolved already at $T = 1.2T_c$. This is in agreement with earlier calculations, which used $F_1(r, T)$ as a potential [16]. The dramatic changes in the spectral functions are not reflected in the correlation function, which shows only about a 4% enhancement. This is due to the fact that even in the absence of bound states the spectral function is enhanced in the threshold region. The enhancement near the threshold occurs because the interaction between the quark and

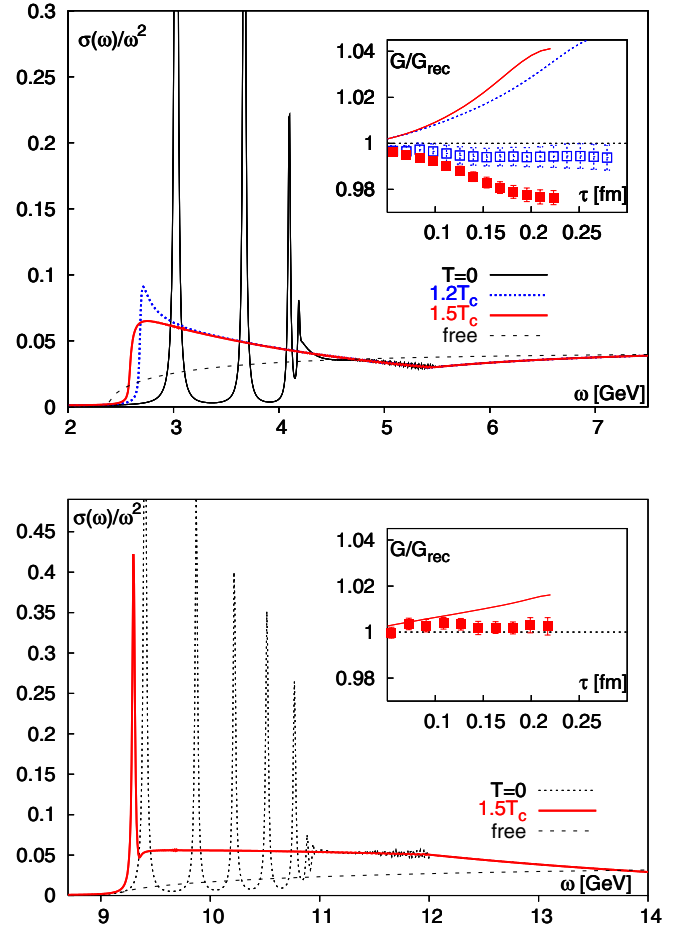


FIG. 6 (color online). The charmonium (top) and bottomonium (bottom) spectral functions at different temperatures calculated using $F_1(r, T)$ as a potential. The insets show the corresponding ratio G/G_{rec} together with the results from anisotropic lattice calculations [30]. G/G_{rec} for charmonium lattice data are shown at two temperatures $T = 1.2T_c$ (open squares) and $1.5T_c$ (filled squares), while for bottomonium lattice data at $1.5T_c$ are shown.

antiquark is still important at this temperature. Even if the potential is assumed to be equal to its lower limit the correlation function does not decrease as expected in the noninteracting case. In Fig. 6 (bottom) we also show the bottomonium spectral function and the corresponding correlators. The ground state bottomonium survives as a resonance up to temperatures as high as $1.5T_c$. However, due to the shift in the peak position, the correlation functions at this temperature get enhanced, resulting in a small increase in the ratio G/G_{rec} . The observed enhancement of G/G_{rec} is clearly incompatible with lattice data [28,30] (see Fig. 6). The analysis of Ref. [62] which uses the free energy as a potential finds the melting of charmonium $1S$ states at $1.2T_c$.

We have also calculated the spectral function and the correlation functions in the scalar channel. The scalar spectral functions show no resonancelike structure above the deconfinement temperatures meaning that all P -wave quarkonia are dissolved. The interactions between the heavy quark and antiquark lead to large enhancement of the spectral functions, similar to the one observed in the pseudoscalar channel. In Fig. 7 we show the ratio of the derivatives with respect to τ of $G(\tau, T)$ and $G_{\text{rec}}(\tau)$ for charmonium and bottomonium at $T = 1.5T_c$. Similar results have been obtained at other temperatures. Our calculations agree quite well with lattice results within their rather large statistical errors. We see again that the large enhancement of the spectral function near the threshold compensates for the dissolution of quarkonium states, leaving the correlation function almost unchanged. Thus, contrary to statements made in Refs. [25,30], the dissolution of the $1P$ quarkonium states does not lead to a large change in the correlation functions. The weak temperature dependence of $G'(\tau)/G'_{\text{rec}}(\tau)$ was first pointed out in Ref. [51]. As we will see in Sec. V, the large change in

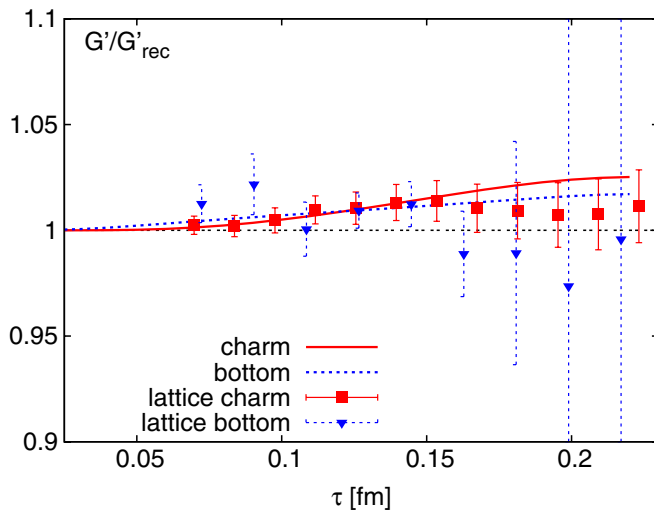


FIG. 7 (color online). The ratio $G'(\tau)/G'_{\text{rec}}(\tau)$ in the scalar channel for charmonium and bottomonium at $T = 1.5T_c$. Also shown are the lattice data for this ratio from Ref. [30].

the P -wave correlators observed in Refs. [25,30] is due to the zero-mode contribution.

D. Numerical results with the potential $V(r, T)$

In this subsection we discuss numerical results from our analysis using the potential $V(r, T)$ discussed in subsection IV B. First, we present the pseudoscalar channel. The charmonium and bottomonium spectral functions at different temperatures are shown in Fig. 8 (top and bottom, respectively). Charmonium spectral functions look similar to the ones discussed in the previous subsection. There are no resonancelike structures in the spectral

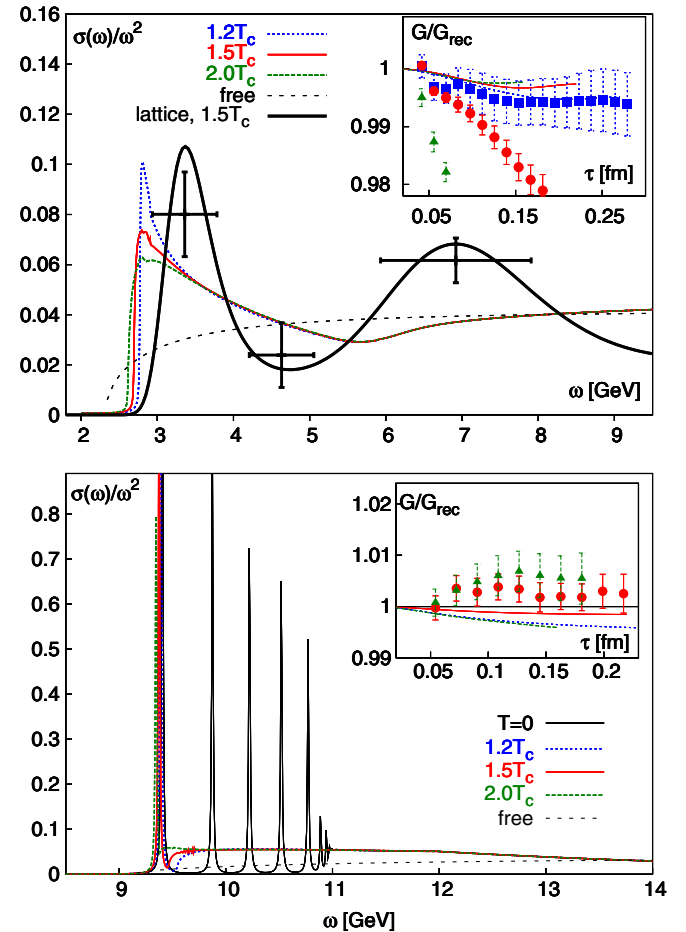


FIG. 8 (color online). The charmonium (top) and bottomonium (bottom) spectral functions at different temperatures calculated using $V_1(r, T)$ as the potential. For charmonium we also show the spectral functions from lattice QCD obtained from the MEM at $1.5T_c$. The error bars on the lattice spectral function correspond to the statistical error of the spectral function integrated in the ω -interval corresponding to the horizontal error-bars. The insets show the corresponding ratio G/G_{rec} together with the results from anisotropic lattice calculations [30]. For charmonium, lattice calculations of G/G_{rec} are shown for $T = 1.2T_c$ (squares), $1.5T_c$ (circles), and $2.0T_c$ (triangles). For bottomonium lattice data are shown for $T = 1.5T_c$ (circles) and $1.8T_c$ (triangles).

function; only a large threshold enhancement. This seems to contradict the conclusions made in Refs. [23–25], where the analysis of the spectral function using the MEM indicated that the first peak survives. A more detailed analysis of the spectral functions in Ref. [30] resulted in the more modest conclusion that within numerical accuracy no significant temperature dependence in the pseudoscalar charmonium spectral functions can be seen. While charmonium spectral functions can be reliably reconstructed at zero temperature using the MEM, this becomes more difficult at finite temperature due to the fact that the extent of the Euclidean time is limited to $1/T$ [30].

To understand the situation better, in Fig. 8 we show our results with the lattice charmonium spectral function of Ref. [30] (solid black curve). The first bump in the spectral function calculated on the lattice is fairly broad and therefore its interpretation as the $1S$ charmonium state is not obvious. The fact that the bump is centered at $\omega \simeq 3.5$ GeV instead of the expected $\omega \simeq 3$ GeV is a systematic effect. It has been observed that also at zero temperature, the position of the first peak is shifted toward larger ω when the extent of the Euclidean time used in the analysis is limited to small values of about $\tau_{\max} = 0.25\text{--}0.3$ fm [30]. Lattice calculations show, however, that the area under the bump does not change within the statistical errors above the deconfinement temperature. More precisely, the spectral function integrated from 2.7 GeV to 4.5 GeV does not change between $T = 0$ and $1.5T_c$. We also calculated in our model the integrated spectral function in this interval and have found a change of about 5%. Note that the spectral function calculated on the lattice has large statistical errors. Thus, it is likely that given the statistical accuracy of existing lattice data on Euclidean correlators the MEM cannot distinguish between a threshold enhancement and a true resonancelike structure in the spectral function at finite temperature.

In the case of the bottomonium we see only the ground state above the deconfinement temperatures, all other states are dissolved. In comparison with calculations discussed in the previous subsection, we see that the medium modifications of the first peak are smaller. This is because the potential $V(r, T)$ is deeper than the singlet free energy (cf. Fig. 5).

In the insets in Fig. 8 we also display the ratio G/G_{rec} which shows a much better agreement with the lattice data compared to the calculations with F_1 discussed above. The deviations between the lattice data and the results of our calculations in the charmonium case for G/G_{rec} are less than 2% for temperatures $T \leq 1.5T_c$. As the temperature is further increased lattice calculations show that G/G_{rec} decreases monotonically [25,30]. At $T = 3T_c$ its value is about 0.9. However, we do not see such a large decrease in our calculations. We expect that this discrepancy is due to the breakdown of the nonrelativistic approximation. As the temperature is increased the charmonia bound states are

melted and therefore the typical velocity of heavy quarks becomes of the order of the thermal velocity $\sqrt{T/m_c}$. At $T = 2T_c$ it becomes $v \simeq 0.7$. Thus the nonrelativistic approximation breaks down and the simple ansatz for the nonrelativistic spectral function given by Eq. (27) is no longer valid. As the temperature is increased beyond this point we expect that the spectral function should slowly approach the free continuum form (30) and thus the ratio G/G_{rec} should decrease (recall Fig. 4). We would expect that for bottomonium the nonrelativistic approximation should be valid at higher temperatures and therefore the calculated ratio G/G_{rec} should agree better with the corresponding lattice data. Results in Fig. 8 show that this is indeed the case.

E. Other choices of the potential

The choice of the potential discussed above is somewhat ambiguous. Given the values of $r_{\text{med}}(T)$ and $V_{\infty}(T)$ there are many ways to interpolate smoothly between the short and long distance regimes. We tried different interpolations and found that the spectral functions do not depend on the method used. Next, one can ask how the results depend on the value of $V_{\infty}(T)$. The free energy $F_{\infty}(T)$ gives a lower bound on this quantity because of the negative entropy term, and the internal energy $U_{\infty}(T)$ provides an upper bound. Therefore we use the singlet internal energy calculated in Ref. [63] as a potential. This quantity has often been used as a potential when discussing quarkonium properties at finite temperature [19–21]. The details of the calculations are discussed in Appendix D. We find that at $1.2T_c$ the $1S$ charmonium and $2S$ bottomonium states are present as resonances in the spectral functions. At higher temperature, of about $T = 1.4T_c$, the only resonant structure which is present is the $1S$ bottomonium state. We also see that the properties of the ground state are significantly modified for this choice of the potential. As a consequence, the temperature dependence of the charmonium correlators does not agree with the lattice results. We also find significant deviation in the bottomonium correlators at $2T_c$. Thus the singlet internal energy is not a reasonable choice for the potential.

The value of $r_{\text{med}}(T)$ in the above analysis was chosen according to the analysis of the singlet free energy. There are many states which contribute to the singlet free energy. As such, the onset of a temperature dependence in the free energy at some distance does not necessarily imply a strong temperature dependence for the potential. However, $r_{\text{med}}(T)$ should be smaller than the distance where we see exponential screening. Therefore, we take $r_{\text{med}}(T) = 1.25/T$ as the upper bound on $r_{\text{med}}(T)$. This gives $r_{\text{med}} \simeq 0.7$ fm at $1.2T_c$ and $r_{\text{med}} \simeq 0.5$ fm at $1.5T_c$. The numerical results obtained from the potential constructed with these values of r_{med} are discussed in Appendix D. We see, in particular, that with such a choice for the potential the peaks corresponding to $1S$ charmo-

nium, $1P$ bottomonium, and $2S$ bottomonium resonances are present and unchanged in the spectral function. The binding energy of these states, i.e. the distance between the resonance peak and the continuum, are quite small. Therefore thermal fluctuations can destroy these states. At $1.5T_c$ we do not see any resonancelike structures, except the $1S$ bottomonium state. Therefore we see that for all choices of the potential which are consistent with the information on color screening coming from lattice QCD, all quarkonium states, except the $1S$ bottomonium, are dissociated at temperatures equal or smaller than $1.5T_c$.

In addition, we have studied quarkonium spectral functions using potentials which are different from the ones mentioned above. A common feature of all the potentials is that they have the same short distance behavior. From the discussion in the previous two subsections it is clear that the strong threshold enhancement is due to the short distance behavior of the potential. The long distance part, however, is different. Here we do not use lattice data to constrain the long distance behavior of the potential. The details of the analysis are given in Appendix D. The quarkonium correlators obtained with these potentials also show a weak temperature dependence. More precisely, we find that $G(\tau)/G_{\text{rec}}(\tau)$ in the pseudoscalar channel and $G'(\tau)/G'_{\text{rec}}(\tau)$ in the scalar channel are temperature independent and are close to unity. Thus the temperature dependence of the correlators does not depend strongly on the details of the potential.

V. ZERO-MODE CONTRIBUTION TO QUARKONIUM CORRELATORS

So far, when addressing the scalar channel we have discussed only the derivatives of quarkonium correlators. The reason for this is the presence of a zero-mode contribution at finite temperature, i.e. there is an extra finite temperature contribution at $\omega \simeq 0$ in the quarkonia spectral function

$$\sigma_i(\omega, T) = \sigma_i^{\text{high}}(\omega, T) + \chi_i^s(T)\omega\delta(\omega). \quad (34)$$

Here $\sigma_i^{\text{high}}(\omega)$ is the high energy part of the quarkonium spectral function discussed in the previous sections, i.e. the one at $\omega > 2m_{c,b}$ and $i = sc, vc, ax$ for the scalar vector and axial-vector channels, respectively. For the vector channel this has been discussed in Refs. [32,64]. In the interacting theory the delta function is smeared and has a Lorentzian form with the width η determined by the heavy quark diffusion constant D , i.e. $\eta = T/M/D$ [64]. For values of D which are not too small the contribution of the second term in the above equation to the Euclidean correlator is given by a constant $G_i^{\text{low}}(T) = T\chi_i^s(T)$. The susceptibilities $\chi_i^s(T)$ have been calculated in the free theory in Ref. [35] and read [65]

$$\chi_{sc}^s(T) = \frac{6}{\pi^2} \int_0^\infty dp p^2 \frac{m_{c,b}^2}{E_p^2} \left(-\frac{\partial n_F}{\partial E_p} \right), \quad (35)$$

$$\chi_{ax}^s(T) = \frac{6}{\pi^2} \int_0^\infty dp p^2 \left(1 + \frac{2m_{c,b}^2}{E_p^2} \right) \left(-\frac{\partial n_F}{\partial E_p} \right), \quad (36)$$

where $E_p = \sqrt{p^2 + m_{c,b}^2}$ and $n_F = 1/(\exp(E_p/T) + 1)$. Adding the constant contribution to the P -wave correlators calculated in the previous section, we can now calculate the ratio G/G_{rec} in the scalar and axial-vector channels. The result of these calculations is shown in Fig. 9 both for charmonium and bottomonium (top and bottom, respectively). Results from isotropic [25] and anisotropic [30] lattice calculations are also displayed. The agreement between our simplified calculations and the lattice data is quite good. Our analysis supports the observation made in Ref. [51] that the large increase in the scalar and axial-vector correlators is due to the low energy contribution to the corresponding spectral functions. One should keep in mind that calculations on anisotropic lattices were done at quark masses which are somewhat heavier than the physical quark masses (cf. Table IIIB). In the bottomonium case we see that there is a quantitative disagreement between the isotropic and anisotropic lattice calculations. This is likely due to the fact that the lattices used in Ref. [30] were too coarse for precise determination of the bottomonium susceptibilities $\chi_{sc,ax}^s(T)$. A constant contribution to the

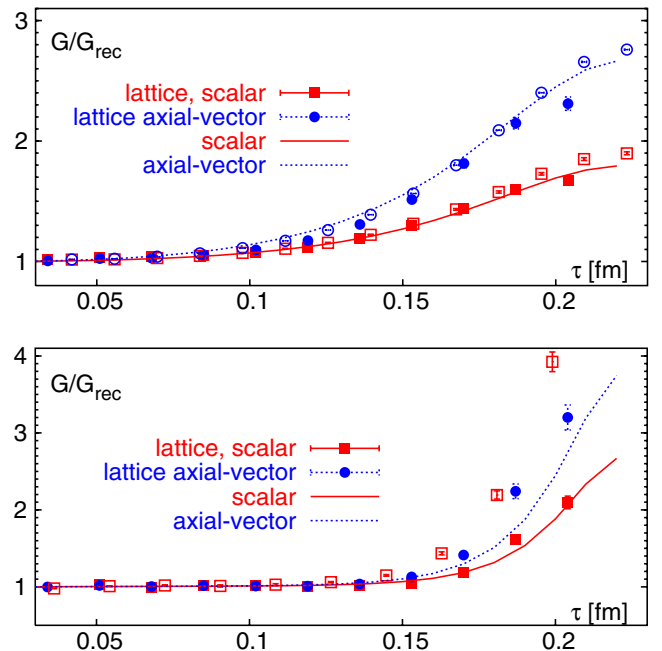


FIG. 9 (color online). The ratio G/G_{rec} in the scalar and axial-vector channel at $T = 1.5T_c$ for charmonium (top) and bottomonium (bottom). Lattice calculation on isotropic lattices [25,28] are shown as filled symbols. Open symbols refer to results from anisotropic lattice calculations of Ref. [30].

correlator $G_i^{\text{low}}(T) = T\chi_i^s(T)$ exists at any nonzero temperature both in the confined and the deconfined phase. In the confined phase the quark number is carried by heavy charm and beauty baryons (remember that here we consider QCD with only heavy quarks) and thus the constant contribution is proportional to $\exp(-3m_{c,b}/T)$. This contribution is very small. In the deconfined phase at sufficiently high temperatures, quark number is carried by quarks and the constant contribution goes like $\exp(-m_{c,b}/T)$, and is described by Eq. (36), which is much larger. The fact that we are able to explain the behavior of the scalar and axial-vector correlators using the ideal gas expressions for the corresponding susceptibilities (Eq. (36)) implies that already at temperatures around $1.5T_c$, the deconfined charm and bottom quarks carry the quark number. This fact directly supports our observation that almost all quarkonium states are dissociated at this temperature.

VI. DISCUSSION AND CONCLUSIONS

In this paper we have shown that lattice data on quarkonium correlators and spectral functions may not necessarily imply survival of different quarkonium states. We analyzed quarkonium spectral functions by solving the Schrödinger equation for the nonrelativistic Green's function of a heavy quark-antiquark pair. The nonrelativistic Green's function is expected to describe the spectral function at energies close to the threshold. The results of these calculations have been matched to the perturbative form of the spectral functions at high energies. Although this matching is not unambiguous the Euclidean correlation functions are not sensitive to the details of the matching. We have shown that this very simple approach can give a reasonable description of the quarkonium correlators calculated on the lattice.

Let us note that there are several considerations which lead to the identification of the nonrelativistic Green's function with the spectral function. One possibility is to construct an effective theory, the potential NRQCD, where the quark-antiquark pair is the only dynamical field at zero temperature [7,8,10]. Attempts to generalize this approach to finite temperatures were recently discussed in Refs. [66,67]. Bottomonia spectral functions have been calculated in this approach using hard thermal loop perturbation theory resulting in S -wave bottomonia spectral functions which are similar to ours [67]. Another possibility to relate Green's functions to the quarkonia spectral function is to construct an integral equation for the vertex function $\Gamma(p, q)$ as discussed in Sec. II while systematically taking into account medium effects. At sufficiently high temperatures, this can be done using perturbation theory. This certainly has to be investigated in the future.

We calculated quarkonium spectral functions at finite temperature using a class of screened potentials based on lattice calculations of the free energy of the static quark-

antiquark pair. Our analysis shows that independent of the details of the choice of the potential, screening effects lead to dissociation of all quarkonium states with the exception of the $1S$ bottomonium state. In particular, we find that the $1S$ charmonium state dissolves at a temperature below $1.5T_c$, contrary to the statements made in the literature based on different potential model analysis [17–22] as well as on the analysis of lattice spectral functions [23–29]. We have analyzed in detail the temperature dependence of the corresponding Euclidean correlation functions and have shown that with some reasonable choice of the potential, the temperature dependence of the quarkonium correlation functions agrees rather well with the pattern observed in lattice QCD calculations, i.e. the correlation functions show very little temperature dependence. Thus lattice data on quarkonium correlators and spectral functions may not necessarily imply survival of different quarkonium states. This can be explained by the fact that even in the absence of resonances, the spectral function is significantly enhanced in the threshold region compared to the case of free quark propagation. This observation may have interesting consequences for quarkonium phenomenology in heavy ion collisions. It means that a strong correlation between the heavy quark and the antiquark is maintained at all temperatures. The heavy quark-antiquark pair is created in hard processes early in the course of heavy ion collisions and therefore the separation between the quark and antiquark is small so that some of them will form correlated pairs. The above observation implies that the initial correlation between the heavy quark and antiquark can be maintained, to some extent, through the entire evolution of the fireball until hadronization. If so, then a fraction of the correlated quark-antiquark pairs emerging from the hard process can form quarkonium states at hadronization.

In this paper we discussed the correlation functions of local meson operators. In lattice calculations, correlation functions of extended meson operators have also been considered [23,68]. These could provide further information on the fate of quarkonium states at high temperatures. However, it is not straightforward to calculate these correlation functions in our approach. Also the comparison of the lattice data with model calculation is less straightforward, e.g. because of the renormalization issues.

Lattice calculations of the free energy of a static quark and antiquark pair show very strong screening effects [44]. On the other hand, the calculations of the S -wave quarkonium correlators show very little temperature dependence [25,30]. This seemed to be puzzling. In [31,32] an attempt to describe quarkonium correlators in the potential model has been made. In those works the spectral functions consisting of bound state peaks and perturbative continuum has been used, and no agreement with lattice data has been found. The same conclusion has been obtained also in [22] when perturbative continuum has been used. More recently, studies which treat bound and scattering states on

an equal footing were presented [21,22]. In [22] such treatment improved the agreement with lattice in the pseudoscalar channel. In [21] no agreement with lattice has been found, which could be due to the fact that the internal energy of a static quark-antiquark pair has been used as the potential. To obtain agreement with lattice for the P -wave correlators inclusion of the zero-mode contributions are essential [69]. The temperature dependence of the P -wave correlator gives further evidence that most quarkonium states are dissolved above deconfinement. In our present work, for the first time, a quantitative understanding of the temperature dependence of the quarkonium correlators has been obtained within a potential model with screening. We were able to explain the temperature dependence of the ratio $G(\tau)/G_{\text{rec}}(\tau)$, despite the fact that most states are dissolved. Good agreement between the lattice data and the potential model prediction was also reported in Ref. [19]. It is important to understand the differences between our analysis and that of Ref. [19]. First, different quarkonium states were reported to exist in the quark-gluon plasma. In particular the dissociation temperature of the $1S$ charmonium state was reported to be $1.62T_c$ [19]. At this temperature, however, the binding energy is 0.2 MeV ! A state with such a small binding energy cannot be detected in the quark-gluon plasma. Second, the authors assumed that only the ground state contribute to the quarkonium correlation function. A recent analysis of the quarkonium spectral function in lattice QCD does not support this assumption [30]. Third, in [19] the ratio $G(\tau)/G_{\text{rec}}(\tau)$ has been calculated as

$$G(\tau, T)/G_{\text{rec}}(\tau, T) = \frac{K(M_q(T), \tau, T)}{K(M_q(T=0), \tau, T)}, \quad (37)$$

where $M_q(T)$ is the quarkonium mass and $K(\omega, \tau, T)$ is the finite temperature kernel defined in Eq. (28). The above equation, however, does not take into account that the contribution of the bound state is proportional to the square of the wave function at the origin (or the corresponding derivative) which decreases with temperature if screening is present. Thus, in [19] the agreement between the potential model calculations and lattice results is accidental and due to the oversimplified approach to the problem.

The analysis presented here can be extended in different ways. Although the $1S$ bottomonium state seems to survive in the deconfined phase, this does not necessarily mean that direct $Y(1S)$ production in heavy ion collisions is not suppressed. In the quark-gluon plasma, the $1S$ state will have a thermal width due to gluon dissociation, which, due to the reduced binding energy, could be sizable [70]. Clearly, the above analysis can be extended to full QCD. Such an extension is very timely, as new information on screening of static quarks in the quark-gluon plasma becomes available from large scale lattice QCD simulations at almost physical quark masses [57]. Finally, it would be interesting

to extend the analysis to finite spatial momenta. We address these questions in [71].

ACKNOWLEDGMENTS

We are grateful to J. Casalderrey-Solana for his contribution at the early stages of this work, especially for providing the programs for numerical calculations of the nonrelativistic Green's function. We thank F. Karsch, D. Kharzeev, L. McLerran, and P. Sorensen for careful reading of the manuscript and valuable comments. This work has been supported by the U.S. Department of Energy under Contract No. DE-AC02-98CH10886.

APPENDIX A

In this appendix we extend the method developed by Strassler and Peskin in [39] to find, besides the nonrelativistic S -wave, also the P -wave Green's function of a central potential. This method can be used for any potential which is less singular than $1/r^2$.

First, we decompose the Green's function into spherical harmonics:

$$G^{nr}(\vec{r}, \vec{r}', E + i\epsilon) = \sum_{l=0}^{\infty} \sum_{m=-l}^l \frac{g_l(r, r', E + i\epsilon)}{r r'} Y_l^m(\theta, \phi) \times [Y_l^m(\theta', \phi')]^*, \quad (A1)$$

where $g_l(r, r', E + i\epsilon)$ fulfills the Schrödinger equation

$$\left[\frac{d^2}{dr^2} - \frac{l(l+1)}{r^2} + m(E + i\epsilon - V(r)) \right] g_l(r, r', E + i\epsilon) = m\delta(r - r'). \quad (A2)$$

The general solution of this equation can be written as

$$g_l(r, r', E + i\epsilon) = A g_{>}^l(r_{>}) g_{<}^l(r_{<}), \quad (A3)$$

where $g_{<}$, $g_{>}$ are the solutions to the homogeneous equation regular at zero and at infinity, respectively, and $r_{<} = \min(r, r')$, $r_{>} = \max(r, r')$. The constant A is given by the Wronskian $\mathcal{W}(f_1, f_2; r) = (f_1 f_2' - f_1' f_2)|_r$,

$$A = \frac{1}{\mathcal{W}(g_{>}^l, g_{<}^l; r)} \frac{m}{4\pi}. \quad (A4)$$

In order to determine these two solutions we then study the homogeneous solutions of Eq. (A2) in the vicinity of the regular singular point $r = 0$. For any potential $V(r)$ less singular than $1/r^2$ there are two solutions, a regular $g_0^l(r)$ and an irregular $g_1^l(r)$, which behave as

$$g_0^l(r) = r^{l+1} + \dots, \quad (A5)$$

$$g_1^l(r) = \frac{1}{r^l} + \dots \quad (A6)$$

Since $g_0(r)$ close to the origin has the largest degree, we can find a power series solution of the form

$$g_0^l(r) = r^{l+1} \sum_{n=0}^{\infty} a_n r^n. \quad (\text{A7})$$

From this expression we determine the other, linearly independent solution $g_1(r)$ using standard techniques [72]:

$$g_1^l(r) = g_0^l(r) \int^r dr' \frac{1}{(g_0^l(r'))^2}. \quad (\text{A8})$$

These two solutions are, in general, divergent at $r \rightarrow \infty$. Since by construction they are linearly independent, we may write the solutions $g_>^l$ and $g_<^l$ defined in (A3) as linear combinations of $g_0^l(r)$ and $g_1^l(r)$. Since $g_<^l$ must be regular in the origin, we chose

$$g_<^l(r) = g_0^l(r), \quad (\text{A9})$$

$$g_>^l(r) = g_1^l(r) + B^l g_0^l(r), \quad (\text{A10})$$

where B is defined as

$$B^l = -\lim_{r \rightarrow \infty} \frac{g_1^l(r)}{g_0^l(r)}. \quad (\text{A11})$$

In order to determine B we solve the homogeneous version of equation (A2) numerically. The initial conditions for this are determined using Eqs. (A7) and (A8). In particular, we determine Eq. (A7) up to the fifth power and compute $g_0^l(\delta)$, $g_1^l(\delta)$, and their first derivatives at $\delta = 0.01 \text{ GeV}^{-1}$.

The relationship between B^l and the Green's function (for S -wave), or its derivative (for P -wave) is obtained from Eq. (A2) and is

$$\lim_{r, r' \rightarrow 0} \text{Im } G^{nr}(\vec{r}, \vec{r}', E + i\epsilon) = -\frac{m}{4\pi} \lim_{r, r' \rightarrow 0} \text{Im} \frac{g_<^l(r) g_>^l(r')}{r r'} \quad (\text{A12})$$

$$= -\frac{m}{4\pi} \lim_{r \rightarrow 0} \text{Im} \left(\frac{g_1^0(r)}{r} + B^0 \right) = -\frac{m}{4\pi} \text{Im } B^0 \quad (\text{A13})$$

$$\begin{aligned} \lim_{r, r' \rightarrow 0} \text{Im } \vec{\nabla} \cdot \vec{\nabla}' G^{nr}(\vec{r}, \vec{r}', E + i\epsilon) \\ = -\frac{3m}{4\pi} \lim_{r \rightarrow 0} \text{Im} \left(\frac{g_1^1(r)}{r^2} + \frac{1}{r} \frac{dg_1^1(r)}{dr} + 3B^1 \right). \end{aligned} \quad (\text{A14})$$

Thus the problem of obtaining the Green's function or its derivative in the origin is now reduced to obtaining the solutions of the homogeneous equations. Care should be taken though, since the solutions $g_1^l(r)$ always contain terms that introduce divergences as $r \rightarrow 0$. The coefficients of these divergences are determined by the coefficients of the expansions (A7) and (A8). The first two coefficients do not depend on the long range part of the potential, while the others depend on the details of the potential, but can be calculated analytically for a given potential not more divergent than $1/r^2$. Since the first few coefficients are real, the $1/r^n$ -like divergent terms do not contribute to the

imaginary part of the Green's function. The divergence of the type $g_0^l(r) \ln r$ in the case of the S -waves is also real and thus it will not enter in (A12). For P -waves, however, the coefficient of the $\ln r$ term in (A14) has also an imaginary part proportional to ϵ . Since the width of the quark can be with good approximation taken to be zero, we can take the limit of $\epsilon \rightarrow 0$, removing this way the divergence that would otherwise enter the imaginary part. In the numerical analysis, where we do have a finite width, we solve this problem by explicitly subtracting the divergence, which we compute from the behavior of $g_1^l(r)$ near the origin. The exact form of such terms depends on the exact form of the potential.

APPENDIX B

In this Appendix we give further details on the comparison of the Euclidean correlators calculated in our model to

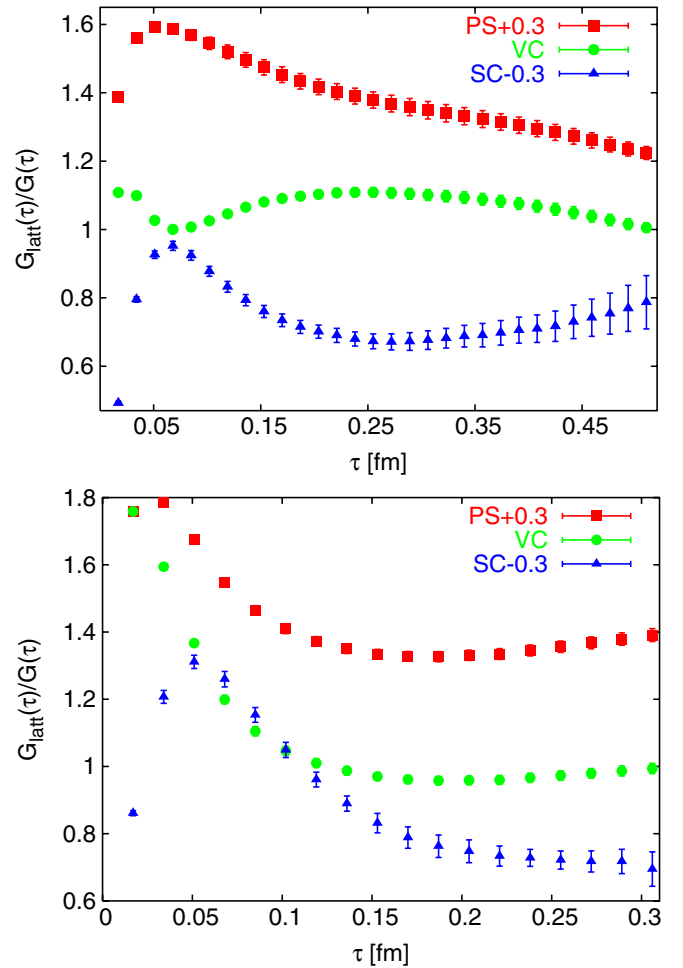


FIG. 10 (color online). The ratio of the correlators calculated on isotropic lattice for charmonium [25,47] (top) and bottomonium [28] (bottom) to the model calculations in the pseudoscalar, vector, and scalar channels. The data in the scalar and pseudoscalar channel have been shifted by ∓ 0.3 for better visibility.

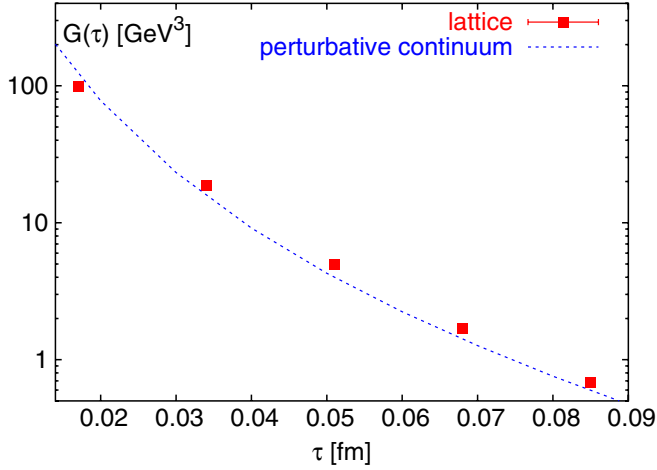


FIG. 11 (color online). The pseudoscalar charmonium correlator calculated on the lattice with subtracted resonance contribution compared to the free continuum correlator.

those from isotropic lattices [25,28,47]. Since the correlation function decays very rapidly with increasing τ (see Fig. 3), in Fig. 10 we show instead the ratio of the Euclidean correlation functions calculated on the lattice and in our model for both charmonium and bottomonium channels. In the charmonium case the model is capable of describing the lattice data within about 10% accuracy for $\tau > 0.2$ fm. This is reasonable, as the validity of nonrelativistic approximation is marginal in this case. At smaller separations lattice data deviate from the model prediction by about 30%. This is expected due to the lattice artifacts discussed in Ref. [34]. For bottomonium we have a similar agreement between the lattice data and model calculations which extend to smaller τ . The reason for this is that the relativistic continuum part of the spectral function is less important for bottomonium, and it becomes visible only at smaller Euclidean time separations. Note that the agreement between the lattice data and model calculations in the pseudoscalar bottomonium correlator could be improved by fine-tuning the K -factor. However, for $\tau < 0.1$ fm the discrepancy between our model calculations and the lattice data is larger than for charmonium. This is understood, because the $\mathcal{O}(ma)$ discretization errors are significantly larger for bottomonium.

We would like to stress again that at sufficiently small τ the relativistic continuum part of the spectral function is important. To demonstrate this point better we have subtracted the contribution of the first and second peaks in the lattice data using the spectral function reconstructed with

the MEM and compared the subtracted correlator to the one obtained from the free relativistic spectral function. This is shown in Fig. 11. We find a reasonable agreement between the free relativistic correlators and the lattice data.

APPENDIX C

In this appendix we discuss the details of constructing the potential $V(r, T)$. It has the following behavior in the short, intermediate, and long distance regimes:

$$V(r) = \begin{cases} V_0(r) = -\frac{\pi}{12} \frac{1}{r} + \sigma r, & r < r_0 = r_{\text{med}} \\ g(r) = g_1 + \frac{g_2}{1 + \exp(\frac{-r + g_3}{g_4})} + g_5 r, & r_{\text{med}} < r < r_1 \\ V_1(r) = V_\infty - \frac{4}{3} \frac{\alpha_1}{r} e^{-\sqrt{4\pi\tilde{\alpha}_1} T r}, & r > r_1 \end{cases} \quad (\text{C1})$$

with $V_\infty = V(r \rightarrow \infty) = \sigma \cdot r_{\text{med}}(T)$. Furthermore we have

$$r_0 = \frac{0.43 \text{ fm}}{T_{\text{red}}} \quad \text{and} \quad r_1 = \frac{1.25}{T}, \quad T_{\text{red}} = T/T_c. \quad (\text{C2})$$

The four parameters $g_1, g_2, g_3,$ and g_4 we chose such that the value of the function $g(r)$ and of its derivative is equal to the value of $V_0(r)$ ($V_1(r)$) and the corresponding derivative at $r = r_{\text{med}}$ ($r = r_1$). Their numerical values are given in Table III. The value of g_5 is zero at $T = 1.5T_c, 2.0T_c$, while $g_5 = 0.00689804$ at $T = 1.2T_c$. Now we can write the potential for arbitrary r as

$$V(r) = f_0(r)V_0(r) + (1 - f_0(r))f_1(r)g(r) + (1 - f_1(r))V_1(r), \quad (\text{C3})$$

where $f_i(r) = \frac{1}{1 + \exp(\frac{r - r_i}{\delta})}$ with $r_i = r_0, r_1$. We choose $\delta = 0.001$.

APPENDIX D

In this appendix we discuss how our results on quarkonium spectral functions and correlators depend on the choice of the potential. First, we use the internal energy $U_1(r, t)$ of the static quark-antiquark pair calculated in Ref. [63] as the potential. We fit the lattice data with the following ansatz

$$V(r, T) = -\frac{\alpha}{r} e^{-\mu r^2} + \sigma r e^{-\mu r^2} + V_0(1 - e^{-\mu r^2}). \quad (\text{D1})$$

The fit parameters are given in Table IV. In addition we use a potential given by Eq. (24) for different values of the

TABLE III. The numerical values of parameters which determine the potential $V(r, T)$.

T/T_c	r_0 [fm]	r_1 [fm]	α_1	$\tilde{\alpha}_1$	g_1	g_2	g_3	g_4
1.2	0.358333	1.042	1.25	0.5	-2.601	2.982	0.0585	0.0989
1.5	0.2866	0.833	0.9	0.45	-17.63	17.94	-0.234	0.113
2.0	0.215	0.625	0.63	0.35	-1.058	1.292	0.0813	0.0903

TABLE IV. The values of the parameter for different sets of the potential used in our analysis.

	T/T_c	μ [GeV]	σ [GeV ²]	V_0 [GeV]
set I	1.13	0.161	0.087	1.094
	1.40	0.408	0.000	0.608
	1.95	0.891	0.000	0.422
	T/T_c	μ [GeV]	r_0 [fm]	V_0 [GeV]
set II	1.2	0.708	0.7	0.47
	1.5	0.885	0.5	0.2
set III	1.2	0.281	0.7	0.27
	1.5	0.394	0.5	0.2
set IV	1.2	0.354	0.557	0.15
	1.5	0.4425	0.445	0.10
set V	1.2	0.354	0.40	0.02
	1.5	0.4425	0.32	-0.02
set VI	1.2	0.704	0.40	0.03
	1.5	0.885	0.32	-0.07

parameters r_{med} , μ , and V_0 and $\alpha' = \alpha$, $\sigma' = \sigma$. We have analyzed five different sets of parameters labeled as II–VI, since the internal energy is labeled as set I. For set II we set $\mu = \mu(T) = 2T$ as predicted by the lattice QCD and $r_{\text{med}} = 1.25 \text{ fm}/(T/T_c)$, i.e. we identified $r_{\text{med}}(T)$ with the distance where screening becomes exponential (see Sec. IV B). We used the same r_{med} in set III but $\mu(T) = 1/r_{\text{med}}(T)$. In parameter sets IV and V we used $\mu = T$, while in the parameter set VI we used $\mu = 2T$. The numerical values of r_{med} , μ , and V_0 for the five different sets are given in Table IV. In Fig. 12 we show the different choices of the potentials, including the free energy $F_1(r, T)$ and the potential $V(r, T)$ discussed in Sec. IV, the internal energy, and the screened Cornell form for the two different

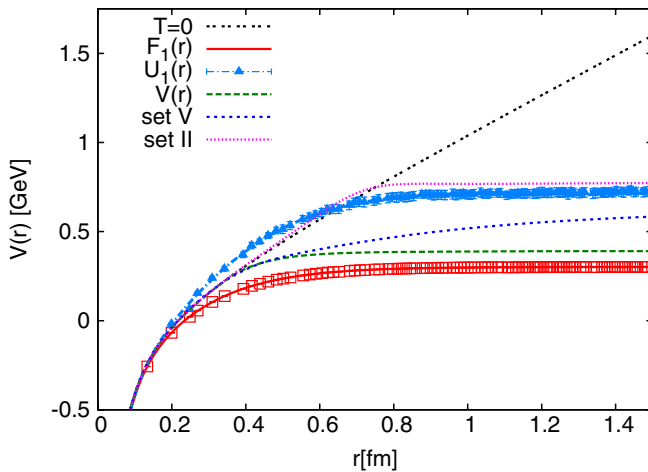


FIG. 12 (color online). Different potential used in the analysis at $1.2T_c$. Triangles correspond to lattice data on internal energy from Ref. [63], while open squares correspond to lattice data on the free energy [53].

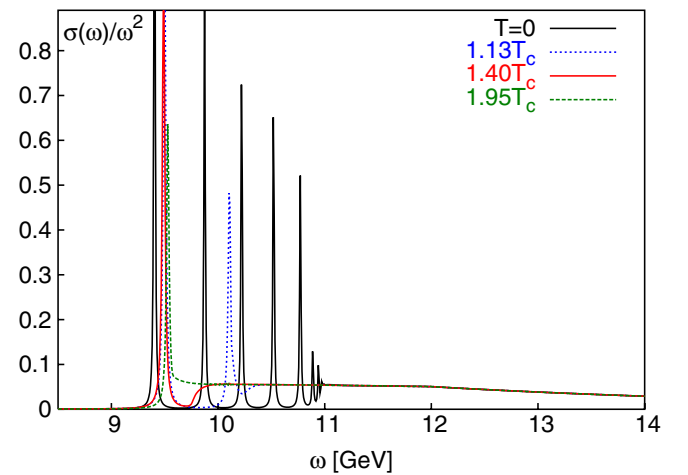
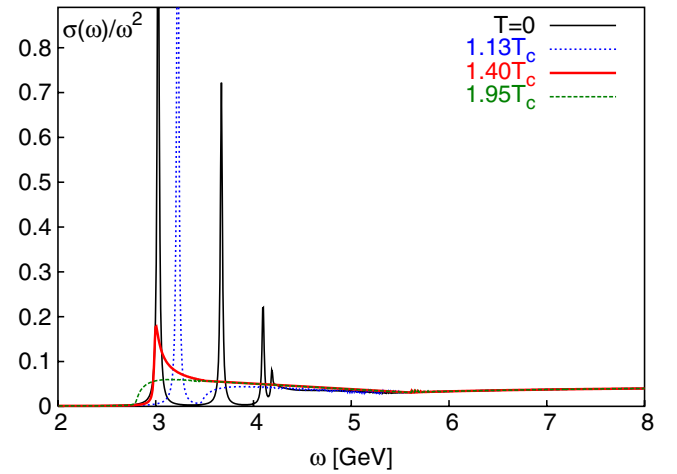


FIG. 13 (color online). Charmonium (top) and bottomonium (bottom) spectral functions calculated using the internal energy as a potential.

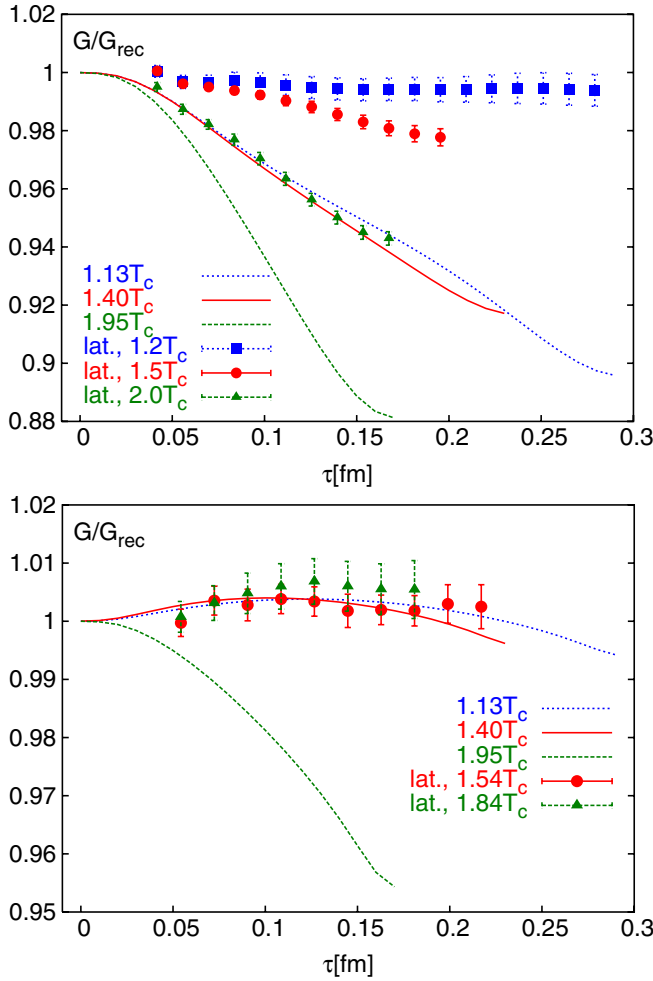


FIG. 14 (color online). The ratio G/G_{rec} for charmonium (top) and bottomonium (bottom) calculated using the internal energy as a potential.

parameter sets at temperatures of about $T = 1.2T_c$. Below we discuss our numerical results for the internal energy and different screened Cornell potentials. The quarkonium spectral functions calculated using the internal energy as a potential are shown in Fig. 13. We see significant increase in the mass and the amplitude of the $1S$ state at the lowest temperature for charmonium and all temperatures in the case of bottomonium. The $1S$ charmonium states dissolve at temperatures around $1.4T_c$, while the corresponding bottomonium states exist up to temperatures of about $2.0T_c$. The temperature dependence of the correlators is shown in Fig. 14. As one can see in the figure, the ratio G/G_{rec} for charmonium is significantly smaller than unity for all temperatures. In the bottomonium case G/G_{rec} drops below 0.96 in contrast to lattice data. The agreement between the lattice data and potential model calculations is worse if we use the internal energy as a potential. The quarkonium spectral function for the parameter set II is shown in Fig. 15. As mentioned above the value of $r_{\text{med}}(T)$ for this parameter set is about its maximal possible value

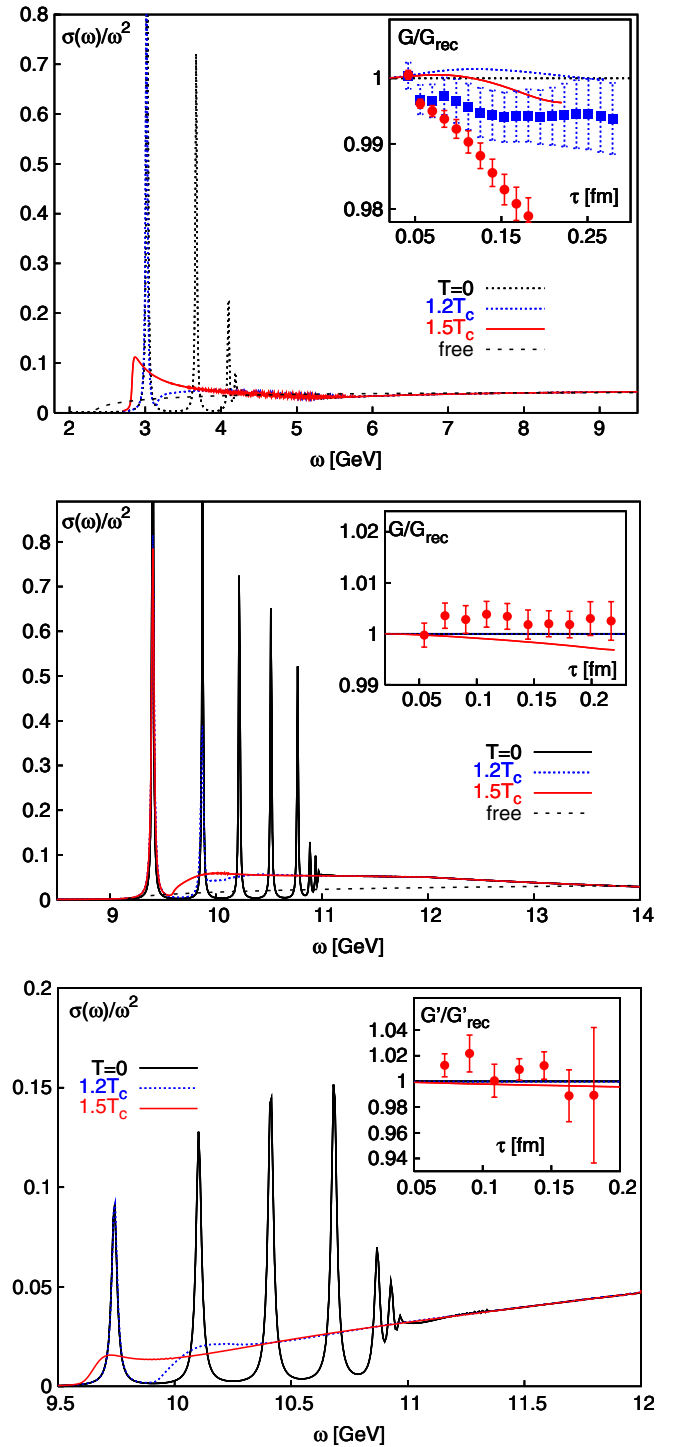


FIG. 15 (color online). The pseudoscalar spectral for charmonium (top) and bottomonium (middle) as well as the scalar spectral function for the bottomonium (bottom) calculated using the potential corresponding to set II. In the insets we show G/G_{rec} as well as G'/G'_{rec} for the scalar channel. Also shown there are the lattice results from Ref. [30] at $1.5T_c$. In the case of charmonium we also show lattice data at $1.2T_c$ (filled squares).

and $\mu = 2T$ as suggested by lattice QCD. Therefore quarkonium states can survive to higher temperatures and

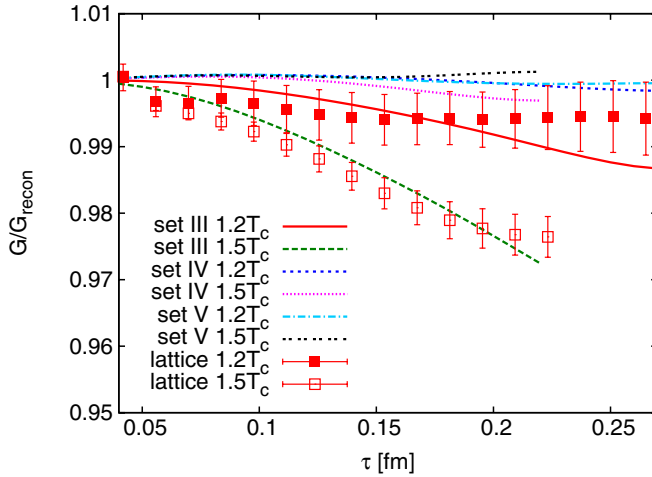


FIG. 16 (color online). The ratio G/G_{rec} for pseudoscalar charmonium for different choices of the potential.

have larger binding energies for this choice of the potential. In this way we can obtain some kind of upper bound on the dissociation temperatures and binding energies for different states. We can see from Fig. 15 that the $1S$ charmonium

state as well as $2S$ and $1P$ bottomonium states survive until temperatures as high as $1.2T_c$ for this choice of the potential. However, the corresponding binding energies are small and therefore interactions with the medium will result in a sizeable thermal width and will lead to the dissociation of these states at this temperature. At higher temperature, namely $T = 1.5T_c$ we no longer see peaks in the spectral functions corresponding to these states. Thus the charmonium $1S$ state and bottomonium $1P$ and $2S$ states are dissolved at temperatures $1.2T_c < T < 1.5T_c$ for this potential. In Fig. 15 we also show the ratio G/G_{rec} for the pseudoscalar channel and G'/G'_{rec} for the scalar channel. One can see that this ratio is close to 1 also for this potential.

We analyzed the spectral functions for other choices of the potential summarized in Table IV and calculated the ratio G/G_{rec} which is shown in Fig. 16 for pseudoscalar charmonium. We see that for all potentials we have studied this ratio is close to unity. Similar results have been obtained for pseudoscalar bottomonium. In the scalar channel we have found the ratio G'/G'_{rec} is also close to unity.

-
- [1] T. Matsui and H. Satz, Phys. Lett. B **178**, 416 (1986).
 [2] E. Eichten, K. Gottfried, T. Kinoshita, J. B. Kogut, K. D. Lane, and T. M. Yan, Phys. Rev. Lett. **34**, 369 (1975); **36**, 1276(E) (1976).
 [3] E. Eichten, K. Gottfried, T. Kinoshita, K. D. Lane, and T. M. Yan, Phys. Rev. D **17**, 3090 (1978); **21**, 313(E) (1980).
 [4] E. Eichten, K. Gottfried, T. Kinoshita, K. D. Lane, and T. M. Yan, Phys. Rev. D **21**, 203 (1980).
 [5] W. Buchmüller and S. H. H. Tye, Phys. Rev. D **24**, 132 (1981).
 [6] W. Lucha, F. F. Schoberl, and D. Gromes, Phys. Rep. **200**, 127 (1991).
 [7] A. Pineda and J. Soto, Nucl. Phys. B, Proc. Suppl. **64**, 428 (1998).
 [8] N. Brambilla, A. Pineda, J. Soto, and A. Vairo, Nucl. Phys. **B566**, 275 (2000).
 [9] G. S. Bali, Phys. Rep. **343**, 1 (2001).
 [10] N. Brambilla, A. Pineda, J. Soto, and A. Vairo, Rev. Mod. Phys. **77**, 1423 (2005).
 [11] N. Brambilla *et al.*, arXiv:hep-ph/0412158.
 [12] F. Karsch, M. T. Mehr, and H. Satz, Z. Phys. C **37**, 617 (1988).
 [13] G. Röpke, D. Blaschke, and H. Schulz, Phys. Rev. D **38**, 3589 (1988).
 [14] T. Hashimoto *et al.*, Z. Phys. C **38**, 251 (1988).
 [15] S. Digal, P. Petreczky, and H. Satz, Phys. Lett. B **514**, 57 (2001).
 [16] S. Digal, P. Petreczky, and H. Satz, Phys. Rev. D **64**, 094015 (2001).
 [17] E. V. Shuryak and I. Zahed, Phys. Rev. D **70**, 054507 (2004).
 [18] C. Y. Wong, Phys. Rev. C **72**, 034906 (2005).
 [19] C. Y. Wong and H. W. Crater, Phys. Rev. D **75**, 034505 (2007).
 [20] W. M. Alberico, A. Beraudo, A. De Pace, and A. Molinari, Phys. Rev. D **72**, 114011 (2005).
 [21] D. Cabrera and R. Rapp, Eur. Phys. J. A **31**, 858 (2007); hep-ph/0611134.
 [22] W. M. Alberico, A. Beraudo, A. De Pace, and A. Molinari, Phys. Rev. D **75**, 074009 (2007).
 [23] T. Umeda, K. Nomura, and H. Matsuferu, Eur. Phys. J. C **39S1**, 9 (2005).
 [24] M. Asakawa and T. Hatsuda, Phys. Rev. Lett. **92**, 012001 (2004).
 [25] S. Datta, F. Karsch, P. Petreczky, and I. Wetzorke, Phys. Rev. D **69**, 094507 (2004).
 [26] H. Iida, T. Doi, N. Ishii, H. Suganuma, and K. Tsumura, Phys. Rev. D **74**, 074502 (2006).
 [27] S. Datta, F. Karsch, S. Wissel, P. Petreczky, and I. Wetzorke, arXiv:hep-lat/0409147.
 [28] S. Datta, A. Jakovác, F. Karsch, and P. Petreczky, AIP Conf. Proc. **842**, 35 (2006).
 [29] G. Aarts, C. R. Allton, R. Morrin, A. P. O. Cais, M. B. Oktay, M. J. Peardon, and J. I. Skullerud, Proc. Sci. LAT2006 (2006) 126 [arXiv:hep-lat/0610065]; Nucl. Phys. A **785**, 198 (2007); arXiv:0705.2198.
 [30] A. Jakovác, P. Petreczky, K. Petrov, and A. Velytsky, Phys. Rev. D **75**, 014506 (2007).
 [31] Á. Mócsy and P. Petreczky, Eur. Phys. J. C **43**, 77 (2005).

- [32] Á. Mócsy and P. Petreczky, Phys. Rev. D **73**, 074007 (2006).
- [33] Á. Mócsy, P. Petreczky, and J. Casalderrey-Solana, Nucl. Phys. A **783**, 485 (2007); **A785**, 266 (2007); Á. Mócsy and P. Petreczky, J. Phys. G **32**, S515 (2006).
- [34] F. Karsch, E. Laermann, P. Petreczky, and S. Stickan, Phys. Rev. D **68**, 014504 (2003).
- [35] G. Aarts and J.M. Martinez Resco, Nucl. Phys. **B726**, 93 (2005).
- [36] L.J. Reinders, H. Rubinstein, and S. Yazaki, Phys. Rep. **127**, 1 (1985).
- [37] M.A. Braun, Sov. Phys. JETP **27**, 652 (1968).
- [38] V.S. Fadin and Khoze, JETP Lett. **46**, 525 (1987).
- [39] M.J. Strassler and M. Peskin, Phys. Rev. D **43**, 1500 (1991).
- [40] M. Laine and M. Vepsalainen, J. High Energy Phys. 02 (2004) 004.
- [41] B.A. Thacker and G.P. Lepage, Phys. Rev. D **43**, 196 (1991).
- [42] The relativistic quark field Ψ can be written in terms of nonrelativistic quark and antiquark fields as $\Psi = (\psi, \chi)$. The simplest operator corresponding to scalar meson then is $\chi^\dagger \vec{\sigma} \vec{D} \psi / m$ [41].
- [43] S. Necco and R. Sommer, Nucl. Phys. **B622**, 328 (2002).
- [44] O. Kaczmarek, F. Karsch, F. Zantow and P. Petreczky, Phys. Rev. D **70**, 074505 (2004); **72**, 059903(E) (2005).
- [45] M. Okamoto *et al.* (CP-PACS Collaboration), Phys. Rev. D **65**, 094508 (2002).
- [46] C.T. Davies *et al.*, Phys. Rev. D **50**, 6963 (1994).
- [47] S. Datta and P. Petreczky (unpublished).
- [48] E.J. Eichten and C. Quigg, Phys. Rev. D **52**, 1726 (1995).
- [49] A. Czarnecki and K. Melnikov, Phys. Rev. Lett. **80**, 2531 (1998).
- [50] M. Beneke, A. Signer, and V.A. Smirnov, Phys. Rev. Lett. **80**, 2535 (1998).
- [51] T. Umeda, Phys. Rev. D **75**, 094502 (2007).
- [52] O. Jahn and O. Philipsen, Phys. Rev. D **70**, 074504 (2004).
- [53] O. Kaczmarek, F. Karsch, P. Petreczky, and F. Zantow, Phys. Lett. B **543**, 41 (2002).
- [54] S. Digal, S. Fortunato, and P. Petreczky, Phys. Rev. D **68**, 034008 (2003).
- [55] P. Petreczky and K. Petrov, Phys. Rev. D **70**, 054503 (2004).
- [56] O. Kaczmarek and F. Zantow, Phys. Rev. D **71**, 114510 (2005).
- [57] K. Petrov (RBC-Bielefeld Collaboration), Proc. Sci. LAT2006 (2006) 144 [arXiv:hep-lat/0610041].
- [58] F. Zantow, O. Kaczmarek, F. Karsch, and P. Petreczky, Nucl. Phys. B, Proc. Suppl. **106**, 519 (2002); O. Kaczmarek (unpublished).
- [59] P. Petreczky, Eur. Phys. J. C **43**, 51 (2005).
- [60] Since the scale in this paper is set by $r_0 = 0.5$ fm the value of $r_{\text{med}}(T)$ determined in Ref. [44] to be $r_{\text{med}}(T) = 0.48 \text{ fm}/(T/T_c)$ has been rescaled.
- [61] E. Megias, E. Ruiz Arriola, and L.L. Salcedo, Phys. Rev. D **75**, 105019 (2007).
- [62] D. Blaschke, O. Kaczmarek, E. Laermann, and V. Yudinchev, Eur. Phys. J. C **43**, 81 (2005).
- [63] O. Kaczmarek, F. Karsch, P. Petreczky, and F. Zantow, Nucl. Phys. B, Proc. Suppl. **129**, 560 (2004).
- [64] P. Petreczky and D. Teaney, Phys. Rev. D **73**, 014508 (2006).
- [65] There is a misprint in Eq. (19) of Ref. [35], $(a_H^{(1)} + a_H^{(2)})I_1$ should read $(a_H^{(1)} + a_H^{(3)})I_1$; we thank Edwin Laermann and Gert Aarts for clarifications of this issue.
- [66] M. Laine, O. Philipsen, P. Romatschke, and M. Tassler, J. High Energy Phys. 03 (2007) 054.
- [67] M. Laine, J. High Energy Phys. 05 (2007) 028.
- [68] T. Umeda, R. Katayama, O. Miyamura, and H. Matsufuru, Int. J. Mod. Phys. A **16**, 2215 (2001).
- [69] Since the present paper has been submitted, the role of the zero-mode contribution has been also realized by the authors of [22], who extended their analysis of the scalar, vector, and axial-vector correlators [73].
- [70] D. Kharzeev, L. McLerran, and H. Satz, Phys. Lett. B **356**, 349 (1995).
- [71] Á. Mócsy and P. Petreczky, Phys. Rev. Lett. **99**, 211602 (2007).
- [72] G.B. Arfken and H.J. Weber, *Mathematical Methods for Physicists* (Academic, New York, 2005).
- [73] W.M. Alberico, A. Beraudo, A. De Pace, and A. Molinari, arXiv:0706.2846.